



UNIVERSITY OF  
CAMBRIDGE

Department of Engineering

---

# Backscatter Communication Simulation

---

Part IIB Project Investigating Techniques to Maximise Range using  
Backscatter Communication

Author Name: Kyeong Min Yu

Supervisor: Dr. Michael Crisp

Date: June 2, 2021

I hereby declare that, except where specifically indicated, the work submitted  
herin is my own original work.

*Signed* \_\_\_\_\_ *Kyeong Min Yu* \_\_\_\_\_ *date* \_\_\_\_\_ *June 2, 2021* \_\_\_\_\_

# Backscatter Communication Simulation

Author: Kyeong Min Yu

Supervisor: Dr. Michael Crisp

Magdalene College, University of Cambridge

## Abstract

The number of IoT devices has growing incredibly rapidly with an annual growth rate of 23% between 2016 and 2021 [2]. This rapid growth has been driven by recent advancements in consumer electronics such as 5G technologies, and the demand for research on IoT communication systems is still growing to this day. Existing active radio technologies are known to provide reliable long ranges but consume a lot of power. Backscatter communications (BackCom) which relies on passive reflection and modulation of incident RF waves is often effective in addressing this energy efficiency problem. However, backscatter systems are known to be limited to short transmission ranges. In this project, two investigations were conducted to improve the communication range of backscatter.

In the first part of the project, noise reduction schemes were applied to limit the phase noise created by the Local oscillator (LO) which is a dominant range-limiting factor in backscatter systems. The two methods investigated via an excel spreadsheet model are Range Correlation Effect (RCE) and Harmonic Backscatter. It was found that RCE outperforms Harmonic Backscatter by almost doubling the achievable communication range at a typical minimum receiver SNR required of 6dB.

Chirp-Spread spectrum (CSS) and Direct-sequence Spread spectrum (DS-SS) are widely used Spread-spectrum modulation techniques in radio technologies which is known to be resistive to interference and noise in detection. These spread-spectrum techniques are also known to easily enable multi-user access with good security. CSS uses modulation using a linear chirp which increases continually in frequency over a specified bandwidth. DS-SS uses a long pseudo-random binary sequence to encode each symbol. By Exploiting backscatter in employing these two modulation schemes, signal architectures can be simplified, and power consumptions can be lowered. In the second part of the project, these two backscatter coding schemes were simulated using MATLAB, and their performances were compared. It was found that the DS-SS backscatter coding scheme outperformed CSS by an increase in communication range by a factor of 1.12, which is considered significant given difficulty in increasing the range in backscatter systems.

Further, to investigate the effect of filtering out the higher order harmonic content in the modulated signals created by rapid backscatter switching, a low-pass filter was implemented at the receiver. The effect of filtering the harmonic content was evaluated for both coding schemes. It was found that for both coding schemes, filtering out the harmonic content improved BER performance compared to systems simulated with signals which contained higher order harmonics. The DS-SS backscatter system had a higher susceptibility to harmonics, as the effect of filtering was more significant than in CSS backscatter. For DS-SS, a decrease in almost 2dB SNR (for the same BER of  $10^{-3}$ ) was achieved by filtering, which amounts to a significant improvement in communication range.

Finally, an ultimate backscatter communication design was proposed combining the architectures found optimal in both parts of the project. A pseudo-random binary sequence encoded backscatter system, which exploits RCE is presented. An approximate achievable range of 280m was calculated using the combined design.

# Contents

|   |           |
|---|-----------|
| <b>1 INTRODUCTION .....</b>                           | <b>5</b>  |
| <b>2 THEORY AND LITERATURE REVIEW .....</b>           | <b>6</b>  |
| 2.1 BACKSCATTER THEORY .....                          | 6         |
| 2.2 PHASE NOISE .....                                 | 7         |
| 2.3 RANGE CORRELATION EFFECT .....                    | 9         |
| 2.4 HARMONIC BACKSCATTER .....                        | 10        |
| 2.5 CSS MODULATION .....                              | 11        |
| 2.6 LORA BACKSCATTER .....                            | 11        |
| 2.7 DEMODULATION VIA MATCHED-FILTER .....             | 12        |
| 2.8 PSEUDO-RANDOM BINARY CODING (DS-SS) .....         | 13        |
| <b>3 NOISE REDUCTION SCHEMES .....</b>                | <b>14</b> |
| 3.1 MOTIVATION.....                                   | 14        |
| 3.2 RANGE CORRELATION EFFECT .....                    | 14        |
| 3.3 HARMONIC BACKSCATTER .....                        | 14        |
| 3.4 SYSTEM MODEL AND ASSUMPTIONS .....                | 15        |
| 3.5 RESULTS AND DISCUSSION .....                      | 16        |
| <b>4 EXPLORATION OF BETTER CODING SCHEMES .....</b>   | <b>18</b> |
| 4.1 MOTIVATION.....                                   | 18        |
| 4.2 SYSTEM MODEL .....                                | 19        |
| 4.2.1 System Model and Assumptions.....               | 19        |
| 4.2.2 Harmonic Content and Filtering .....            | 22        |
| 4.3 CSS BACKSCATTER .....                             | 25        |
| 4.3.1 CSS Encoding.....                               | 25        |
| 4.3.2 CSS Decoding.....                               | 26        |
| 4.3.3 BER vs SNR Simulation .....                     | 28        |
| 4.3.4 FSCSS Backscatter .....                         | 31        |
| 4.4 DS-SS BACKSCATTER .....                           | 34        |
| 4.4.1 DS-SS Encoding .....                            | 34        |
| 4.4.2 DS-SS Decoding.....                             | 35        |
| 4.4.3 BER vs SNR Simulation .....                     | 37        |
| 4.5 CSS vs DS-SS DISCUSSION .....                     | 39        |
| <b>5 PROPOSED LONG-RANGE BACKSCATTER SYSTEM .....</b> | <b>41</b> |
| <b>6 CONCLUSION .....</b>                             | <b>43</b> |
| <b>7 FUTURE WORK .....</b>                            | <b>44</b> |
| <b>8 APPENDIX .....</b>                               | <b>46</b> |

---

## 1. Introduction

There has been an ongoing search for wireless technology that can provide reliable and long-range communication at tens of microwatts of power as well as costing only a few cents. Active radio technologies including Wifi, Zigbee, LoRa (Long-Range) and LTE-M provide reliable and long ranges but are very power-consuming, costing 4-6 dollars [2]. As Internet of Things (IoT) is beginning to take a major place in the telecommunication market, Backscatter communication serves as a potential solution in reducing power consumption and manufacturing cost of IoT systems as a low-power, low-complexity technique. It exploits the reflected backscatter signals by using an intermediate tag to transmit data. This is different to traditional communication systems, where the transmit information is included in the incident signal and is delivered to the receiver directly.

While Backscatter is low-power and low-cost, it is known to be limited to short-ranges as it faces problems with noise and interference and a two-way path loss. For a standard backscatter system with a linear tag, the power of the received signal experiences free-space propagation losses twice: once as it travels from the signal source to the backscatter tag, and once again as it travels back to the receiver. The received power cannot be below a certain threshold limited by the receiver sensitivity. As the path loss depends on the communication range, this two-way loss acts as a range-limiting factor.

Further, the noise floor is raised above the thermal limit due to phase noise generated at the Local Oscillator [16], which limits the communication range of backscatter systems. There are various ways to address this limitation on range due caused by noise, and in the project, we explore two noise reduction schemes to reduce this phase noise: Range Correlation Effect (RCE), and Harmonic Backscatter, and validate their effectiveness using spreadsheet modelling.

Traditionally, backscatter tags can allow phase-based modulation schemes, such as PSK, FSK and QAM to add robustness to noise [8] in attempt to improve the communication range. While in conventional radio communication systems, Spread-spectrum techniques are used to add resistance to interference and noise, enable multi-user access and improve security and privacy in transmission. These advanced Spread-spectrum techniques are not yet found to have been often employed successfully to backscatter systems, other than a LoRa CSS backscatter design presented in [1]. Therefore, in the second part of the project, two backscatter coding schemes, Chirp Spread Spectrum (CSS) and Direct-Sequence Spread spectrum (DS-SS) backscatter modulations were simulated using MATLAB, and their performances were compared.

## 2. Theory and Literature Review

### 2.1 Backscatter Theory

A typical backscatter system has three components: the signal source, the backscatter transmitter and the backscatter receiver. The source signal is either generated by a designated signal generator, or is obtained from an ambient RF source such as a cellular base station or a TV tower [2]. This source signal is modulated and reflected at the backscatter transmitter. The receiver then decodes information symbols received from the transmitter. Hence in backscatter, two-way pathloss is involved which limits the transmission range compared to conventional RF systems.

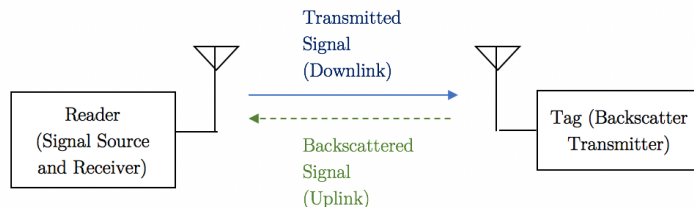


Figure 1. Monostatic Backscatter Communication System

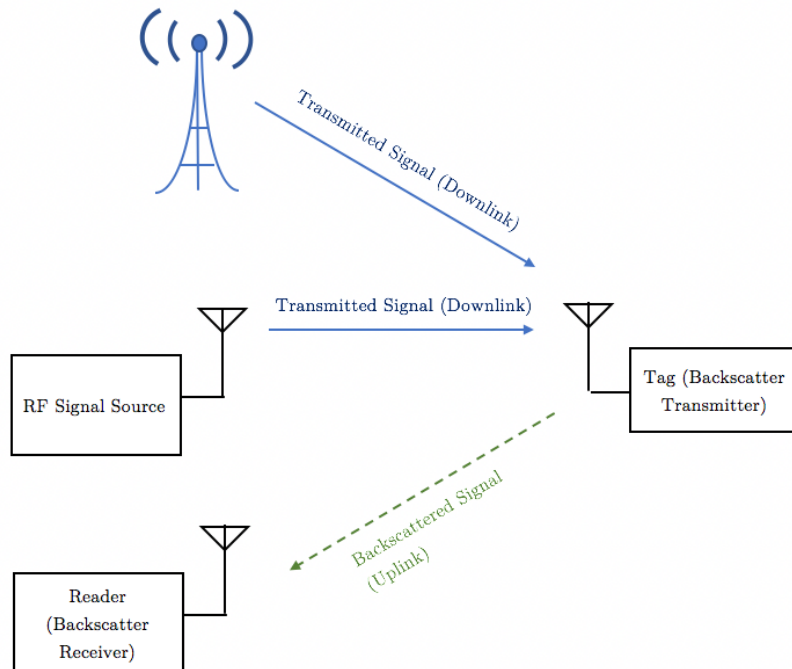


Figure 2. (Ambient) Bistatic Backscatter Communication System

According to the system architectures, backscatter communication can be further categorized into 2 types: Monostatic and Bistatic. In monostatic backscatter as in figure 1, the same device is used for the signal source and backscatter receiver. For

Bistatic Backscatter, the signal source and receiver are at different terminals as in figure 2. The incident signal to the backscatter tag can be from a chosen signal source, or from ambient RF signals; this choice is illustrated in figure 2. One of the advantages of using a designated signal source is that the source can be placed close to the backscatter tag to minimize the pathloss, hence is widely used for RFID applications. On the other hand, ambient backscatter systems usually minimize the cost and increases energy efficiency [2].

Backscatter systems can further be categorized according to whether the tag is active, passive or semi-passive. The active tag has internal power supply, so it can send information actively to the reader actively as well as sending backscattered information. A passive backscatter transmitter has no internal power supply, operating via energy harvesting and sends incident information only if requirements are satisfied. A semi-passive tag performs the functions of both active and passive tags, not sending data actively, but backscattering data only when excited. Monostatic backscatter with a semi-passive or passive tag is most popularly used in RFIDs because of its low cost, low-power simple tag architecture. However, the use of a battery-powered semi-passive tag will give better communication range than using a passive tag.

In backscatter RFID, the emitted signal consists of a single carrier wave produced by a local oscillator. The signal is then transmitted (downlink) and modulated by the tag, then backscattered, transmitted (uplink), and received by the reader. The received signal contains generated sidebands shifted by an offset frequency, with an associated channel bandwidth.

This project aims to investigate and compare different backscatter techniques with the aim of maximizing the communication range, rather than increasing cost or energy efficiency. Therefore, all simulations will be conducted with the assumption of a monostatic backscatter system with a semi-passive tag and a designated signal source to allow simplification of comparisons and simulations.

## 2.2 Phase Noise

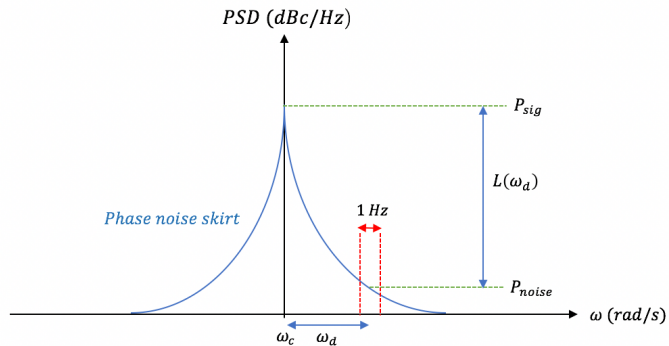


Figure 3. Definition of Phase Noise,  $L(\omega_d)$

$$L(\omega_d) = 10 \log \left( \frac{P_{noise}(\omega_d)}{P_{sig}} \right), \quad [dBc/Hz] \quad (1)$$

One of the major factors which limit the range in a backscatter system is the phase noise produced by the local oscillators (LOs). Generally, the noise produced by LO's have both amplitude and phase, but the amplitude contribution can be ignored as oscillators have their own amplitude regulation ability [16]. This phase noise in the signal is very difficult to filter out [5], while it affects the channel bandwidth and the receiving signal error rate, limiting the communication range.

In direct down conversion receivers, in which a mixer containing a LO converts the incoming signal to a lower frequency, it is easy for phase noise to slip into the signal. While an ideal frequency spectrum at an oscillator output is a spectral line at the carrier frequency, the spectrum in reality has broad phase noise skirts around the carrier frequency,  $\omega_c$ .

Phase noise is defined for a certain offset frequency from the carrier [16], and for a measurement bandwidth of 1Hz. It is a rate of the noise power,  $P_{noise}$  in 1Hz bandwidth at the offset frequency,  $\omega_d$  in the signal power  $P_{sig}$ , as defined mathematically in Equation (1) and illustrated in figure 3. It is defined as the level below the carrier for 1Hz bandwidth, so is always negative in definition.

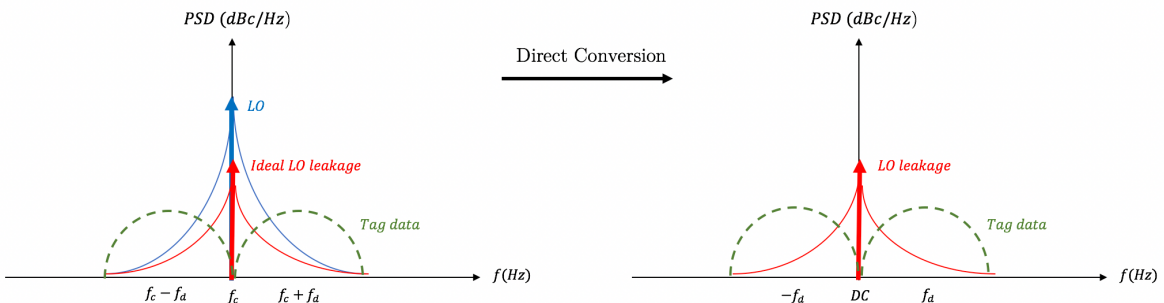


Figure 4. Signal before and after Reciprocal Mixing with two LO's at the reader

The presence of this phase noise skirts influences radar performance in several ways. The phase noise skirts of the leaked LO signal from Tx to Rx masks the desired backscattered signal, making it difficult to decode the received tag data at the receiver. The direct leakage of LO from Tx to Rx is a principal part of the phase noise, and this raises the noise floor well above the thermal limit. The noise floor is further raised by reciprocal mixing of the desired signal, the LO at the receiver and a strong interference signal close to  $f_c$  [24]. In monostatic systems, the phase noise due to reciprocal mixing is severe, as illustrated above in Figure 4.

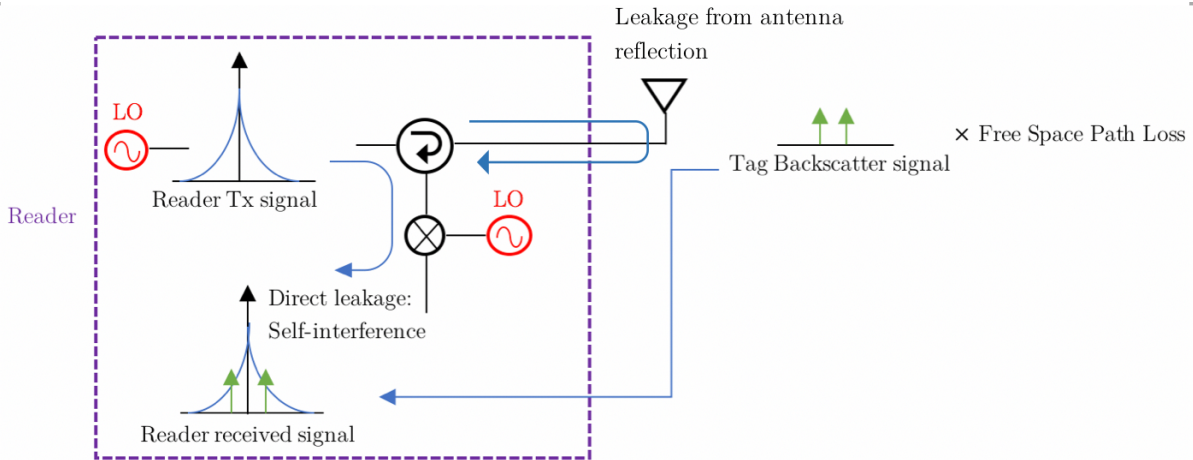


Figure 5. Signal leakage path in a typical Monostatic RFID system with a circulator, and two LO's

Figure 5 illustrates the signal flow of a monostatic backscatter system. In a typical system with a linear backscatter tag, the uplinks and downlinks will be at carrier frequency, causing ‘jamming’ to the receiver due to the desired signal getting buried under the leaked LO phase noise skirts. The two main signal leakages are from the direct leakage from the circulator, and leakage from antenna reflection as shown in blue in the figure. A Circulator is an isolation device that is commonly used to separate the Tx/Rx channels, and can usually provide up to 25-30dB isolation. If the signal leakages are not suppressed well, the noise floor will set by the phase noise skirts of the leaked signal, often more than 90dB than the thermal noise floor [10]. This significantly limits the communication range. Further, system failure may occur by saturation at the receiver.

### 2.3 Range Correlation Effect

From figure 5, it can be seen that a monostatic RFID reader typically comprise of two local oscillators, one for carrier generation, and a second oscillator for the mixer input. When the system architecture is manipulated such that a single LO is used for both purposes, the net phase noise can be significantly reduced. Then, the phase noise of the received signal is correlated with that of the LO signal such that the correlation level is inversely proportional to the time difference between the two signals [24], [4]. In a monostatic RFID system, this time delay is very small due to the short tag-reader distance, significantly reducing the phase noise, which lowers the noise floor. This phase noise reducing effect is called ‘Range Correlation’ in radar applications.

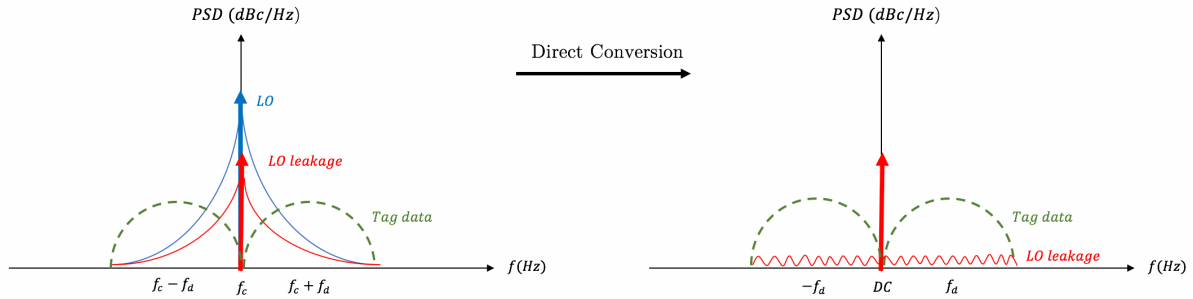


Figure 6. Signal before and after Reciprocal Mixing with Range Correlation Effect

The new phase noise must be calculated by considering both the reciprocal mixing and the phase-noise reduction through the range correlation effect. The paper in [24] studies the range correlation effect on RFID systems in more detail. Figure 6 illustrates the concept of reciprocal mixing with range correlation effect and shows the signal architecture before and after reciprocal mixing. Unlike the system where two LO's are used, with range correlation, the LO noise spectra effectively cancel out, significantly lowering the noise floor.

## 2.4 Harmonic Backscatter

The use of a ‘harmonic’ tag also offers a solution to the issue of the backscattered signal getting buried in the phase noise skirts due to strong leakage. Unlike conventional RFID tags, harmonic tags exploit nonlinear components to passively generate harmonics for the uplink response [10]. The uplink and downlink signals can be carried at different frequencies, separating the Tx and Rx on different bands, reducing Tx-to-Rx interference.

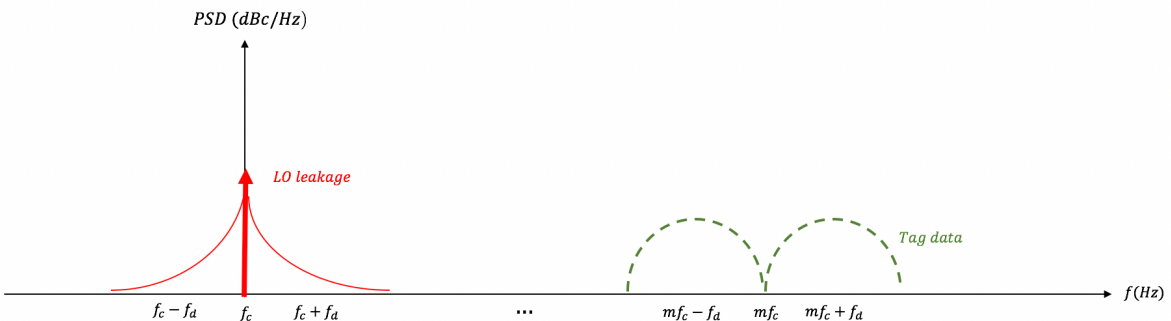


Figure 7. Received Signal at the reader having been reflected by Harmonic Tag

The Self-jamming can be eliminated via nonlinear backscatter as illustrated in Figure 7. The uplink response can be modulated onto the  $m^{th}$  harmonic (usually 2<sup>nd</sup> harmonic), which is passively generated by nonlinear devices at the tag. Then, LPFs and HPFs are used to easily separate the received signal at the reader. Unsurprisingly, due to the large frequency separation which is in the range of GHz, it is not difficult to filter out the two signals. Also, the nonlinear backscatter approach known to be very

flexible in construction and deployment. As a result, the receiver noise floor can be set by the thermal noise floor at -174dBm/Hz rather than the phase noise skirts of the LO leakage signal.

However, power losses are increased with a nonlinear harmonic tag, negatively affecting the achievable communication range. Therefore, there will be a tradeoff between the lowered noise floor and the increased power loss by using harmonic backscatter.

## 2.5 CSS Modulation

Chirp spread spectrum (CSS) communication system uses linear chirps to represent symbols. CSS encodes ‘chirps’ which continually linearly increase or decrease in frequency. CSS makes use of the entire bandwidth allocated which makes it strong against channel noise and interference. Therefore, CSS modulation is often adopted in various long-range wireless applications exploiting its advantages in robustness against narrow-band interference, and resistance against multi-path fading [29].

Historically, and for simpler digital communication applications, CSS is used as a simple form of binary symbol encoding, in which two linear chirps in opposite sweep directions (the up and down chirp) are used to represent Symbols 0 and 1 to be transmitted. The scheme is otherwise known as ‘Slope-Shift Keying’. The data symbols are multiplied with the increasing frequency chirp created at a much higher bit rate, spreading the bandwidth of the actual data. The spread bits are then transmitted at a higher data rate. This method ensures a very low SNR of the received signal, and hence decreases the bit error probability [14].

Further, More recently LoRa technology has been introduced for IoT applications which utilizes frequency-shift chirp modulation (FSCSS). By utilizing different frequency-shifted versions of the linear chirp, FSCSS modulation further reduces receiver complexity low-complexity demodulation using the fast Fourier transform [25], and allows more symbols to be encoded.

In the project, slope shift keying using backscatter is simulated, and will be referred to as CSS for the rest of the report. In **Section 4.3.4**, FSCSS implementation was attempted, although not carried on for further simulation due to problems raised in demodulation.

## 2.6 Lora Backscatter

[1] presents a first long-range backscatter tag design which uses FSCSS encoding scheme compatible with LoRa. In their backscatter device design, a harmonic cancellation mechanism is presented. In contrast to various prior backscatter designs which use square waves to approximate sine waves which results in higher order harmonics in the modulated signal, the design in [1] uses a multi-level signal to approximate sine waves. The backscatter switch mapper with multiple impedance states is exploited for

implementation. This harmonic ‘cancellation’ mechanism avoids the creation of higher order harmonics in the first place in the modulation step using backscatter. This successfully addresses the problem of interference caused by the existence of 3<sup>rd</sup> and 5<sup>th</sup> harmonics which increases difficulty in decoding and limits the range.

The backscatter tag design presented in [1] is used as reference in our system design of our own CSS backscatter design. The harmonic cancelling mechanism method is noted for reference for future work.

## 2.7 Demodulation via Matched Filter

Matched filters are one of the most commonly used time-domain methods in radar systems. A matched filter correlates a known deterministic signal with the received signal in order to maximize the peak output SNR when a noisy signal is passed through it. If the parameters of the noisy signal is known, the optimal detector in Gaussian noise is proven to be a matched filter followed by a threshold comparison [24]. Passing the noisy signal through its corresponding matched filter should result in a high peak at the output. This output is known as the autocorrelation function which is well studied in many applications. For our simulations, this simple matched filtering method is employed for decoding as mathematically described below in Equations (2) to (4).

$$y[n] = \sum_{k=-\infty}^{\infty} h[n-k]x[k] \quad (2)$$

In Equation 3,  $x[k]$  is the input to the matched filter,  $y[n]$  is the matched filtered output, and  $h$  is the impulse response of the linear filter that maximizes the output SNR.

$$x = s + v \quad (3)$$

The observed signal,  $x$  (the actual input to the matched filter) can be written as the sum of the desired signal,  $s$  with added noise,  $v$ .

After long derivation, the form of the linear filter can be derived,

$$h = \frac{1}{\sqrt{s^H R_v^{-1} s}} R_v^{-1} \quad (4)$$

where  $R_v$  is the noise covariance matrix and  $s^H$  denotes the Hermitian.

If the impulse response of the filter is written for a convolution system, the matched filter can be interpreted to be simply the complex conjugate time-reversal of the desired input signal,  $s$ . This interpretation will be used as our method for our matched filter

design model in **Section 4**. This type of matched filter is otherwise known as a ‘correlator’.

## 2.8 Pseudo-random Binary Coding (DS-SS)

Direct-sequence spread spectrum (DS-SS), also called as direct sequence code division multiplexing (DS-CDMA), and is also a type of spread spectrum communication, like CSS. In DS-SS, the data symbols to be transmitted are multiplied by a higher data-rate, larger bandwidth pseudo-random bit sequence (also called ‘chips’). The redundant chips help the signal resist the channel noise and interference and also enables the original data to be recovered if data bits are damaged during the transmission [31]. The transmitted signal is then decoded by correlating the received signal with the same pseudo-noise code used at transmission, using a matched filter followed by a threshold detector.

The Pseudo-noise (PN) code sequence is a sequence of ones and zeros which alternate in a random fashion. The word ‘pseuedo’ is included because it is not entirely random, but is coded with a deterministic algorithm which is repeated for each symbol, and is known to both the transmitter and receiver [29]. In real ‘random’ sequences would be generated entirely by white noise. This gives PN sequences an advantage as it can be easily created and repeated. Pseudo-random number generators (PRNGs) are used to generate the PN sequence, and a typical example used is a Linear congruential generator, which uses recurrence to generate the sequence [32]. Often in CDMA, Gold Codes, Kasami sequences and JPL sequences are used as the PN sequence, and are usually simple to generate and relatively easily synchronized [27].

Theses PN sequences generated are usually difficult to predict, and exhibits statistical behavior similar to a truly random sequence although coded deterministically. The randomness in the sequence gives it good correlation, giving a sharp correlation peak when decoding, giving it robustness to interference. Evidently, improved security can also be achieved via the pseudo-random coding as it is almost impossible to recover the transmitted data without knowledge of the code. Further, DS-SS systems have benefits in enabling multi-user access. Multiple users can transmit simultaneously over a single channel, via allocating a unique PN sequences for encoding for users.

In **Section 4.4**, we explore implementing a pseudo-random coding scheme similar to the DS-SS technique using a backscatter design. Then in **Section 4.5**, we compare the performances of CSS and DS-SS modulation applied to backscatter. Although our assumptions used in designing pseudo-random binary coding scheme has not been cross-checked if it is realistically comparable to DS-SS, for the rest of the report, the random coding scheme will be referred to as DS-SS. We expect the randomness property of DS-SS would give it a sharper correlation peak in detection lowering the BER, making it more robust to noise.

### 3. Noise Reduction Schemes

#### 3.1 Motivation

One of the most important range-limiting factors in backscatter communication is the phase noise being present as well as the desired signal in the received signal, as described in **Section 2.2**. For a common RF source, the phase noise at 100kHz offset is about -110dBc/Hz. Even if the leakage signal is 0dBm, this -110dBm/Hz phase noise is much higher than the thermal noise floor of -174dBm/Hz. For more direct leakage, the desired backscattered signal may be buried in the phase noise skirts.

In receivers, a certain minimum SNR is required for each type of modulation in order that it can be reliably decoded. The phase noise from the leaked signals act as the range limiting factor in monostatic systems, thus it is wished to eliminate this phase noise as much as possible using the two noise reduction schemes below.

#### 3.2 Range Correlation Effect

In RCE, a single LO is used for transmitting, and as the input to the receiver mixer as described in **Section 2.3**. Effectively, two signals that are correlated to each other with a small time delay will be mixed, so that the central phase noise cancels itself, creating a ‘range correlation effect’, reducing the total noise in the received signal. The reduced phase noise using RCE was modelled according to the Equation 5:

$$N_{RC} = N_{\theta_{LO}} * 4\sin^2(\pi\Delta(t)f_o) \quad (5)$$

where  $N_{RC}$  is the new reduced phase noise by RCE,  $N_{\theta_{LO}}$  is the original phase noise from the LO,  $f_o$  the offset frequency and  $\Delta(t)$  the time delay between transmitted and received signals [6].

The new noise floor modelled in the system model is defined using this improved phase noise, with an added an isolation from the circulator and a small noise figure.

#### 3.3 Harmonic Backscatter

In harmonic backscatter systems, the self-interference from the LO is avoided via passively modulating the uplink response to an integer multiple of the carrier frequency at the tag [5] as described in **Section 2.4**. In this project, we consider exploiting the second harmonic, where a non-linear tag is used acting as a frequency doubler. Then, the downlink signal that is carried at  $2f_c$  and the carrier transmit signal at  $f_c$  can easily be separated by using broadband low-pass and high-pass filters at the reader. This process brings down the noise floor down to the thermal noise limit, therefore increasing the range. The noise floor in our simulation is defined as thermal noise of -174dBm/Hz plus a small noise figure.

In a traditional backscatter system with a linear tag, the power of the received tag response,  $P_r$ , experiences free-space propagation losses twice, once each from the downlink and uplink (hence, a ‘two way path loss’). Therefore,  $P_r$  is inversely proportional to the communication distance to the 4<sup>th</sup> power. However, in this harmonic-tag backscatter system, power losses increase at double the rate via the non-linearity of the tag. Unlike the linear relationship between the power in and out at the tag for a normal system, the power out at the tag will be square the input at the tag for the harmonic backscatter model. The rate of change of return power is twice as fast in the harmonic tag. Therefore,  $P_r$  is inversely proportional to the communication distance to the 6<sup>th</sup> power. This is implemented in the simulation by modelling the backscatter transmission loss in the link budget is modelled as a function as the power in at the tag.

The range-maximization will be a compromise between the increased power loss and the lowered phase noise; evaluation on whether the model performs better than a standard model will be investigated via spreadsheet modelling.

### 3.4 System Model and Assumptions

To simulate the effect of exploiting RCE and harmonic backscatter on the performance of maximizing range, excel spreadsheet modelling was used to establish a power budget valuation of the different backscatter models.

Here, monostatic backscatter models were used with other assumptions used as independent variables in the model in Table 1 below. These values were taken from an experiment used in [3].

|  |             |
|--|-------------|
| Transmit Power, $P_T$                      | 29 dBm      |
| Antenna Gain at the receiver, $G_{TR}$     | 7 dB        |
| Antenna Gain at the tag, $G_t$             | 2.1 dB      |
| Backscatter Transmission Loss $T_b$        | -5 dB       |
| Carrier frequency, $f_c$                   | 915MHz      |
| Offset frequency, $f_d$                    | 100kHz      |
| Thermal Noise                              | -174 dBm/Hz |
| Bandwidth                                  | 50kHz       |
| Noise Figure                               | 1.5 dB      |
| Phase Noise for Normal System<br>(Control) | -110 dBc/Hz |
| Polarization mismatch, $X$                 | 1           |
| On-object gain penalty, $\Theta$           | 1           |
| Path blockage loss, $B$                    | 1           |
| Modulation Factor, $M$                     | 1           |
| Monostatic Fade Margin, $F_2$              | 1           |

Table 1. List of Assumptions used for Spreadsheet Modelling

The performance of Harmonic Backscatter and RCE was evaluated by comparison to a typical monostatic backscatter model with a linear tag, which was used as the control. The backscatter link budget from [3] was used for the relationship between transmitted and received powers and communication range, as shown in Equation 6.

$$P_R = \frac{P_T G_{TR} G_t \lambda^4 X^2 M}{(4\pi r)^4 \Theta B^2 F_2} \quad (6)$$

For Harmonic Backscatter, the assumptions given in Table 1 were used except for the backscatter Transmission Loss,  $T_b$ . Rather than using a constant value,  $T_b$  was modelled as a function of the power in at the tag instead, replicating the non-linear tag design. For RCE, all assumptions were used except for the phase noise, which was calculated using Equation 5. For RCE, a time delay of 9ns was used, which was taken from [6].

### 3.5 Results and Discussion

A key plot of link budgets was produced from these models displaying the achievable range of the models given a Transmit Power. The control model and RCE models share the same link budget, and therefore the same plot, shown in orange in figure 8, whereas the Harmonic model produces the steeper link budget plot shown in yellow. The horizontal lines show the limiting noise levels of the three models.

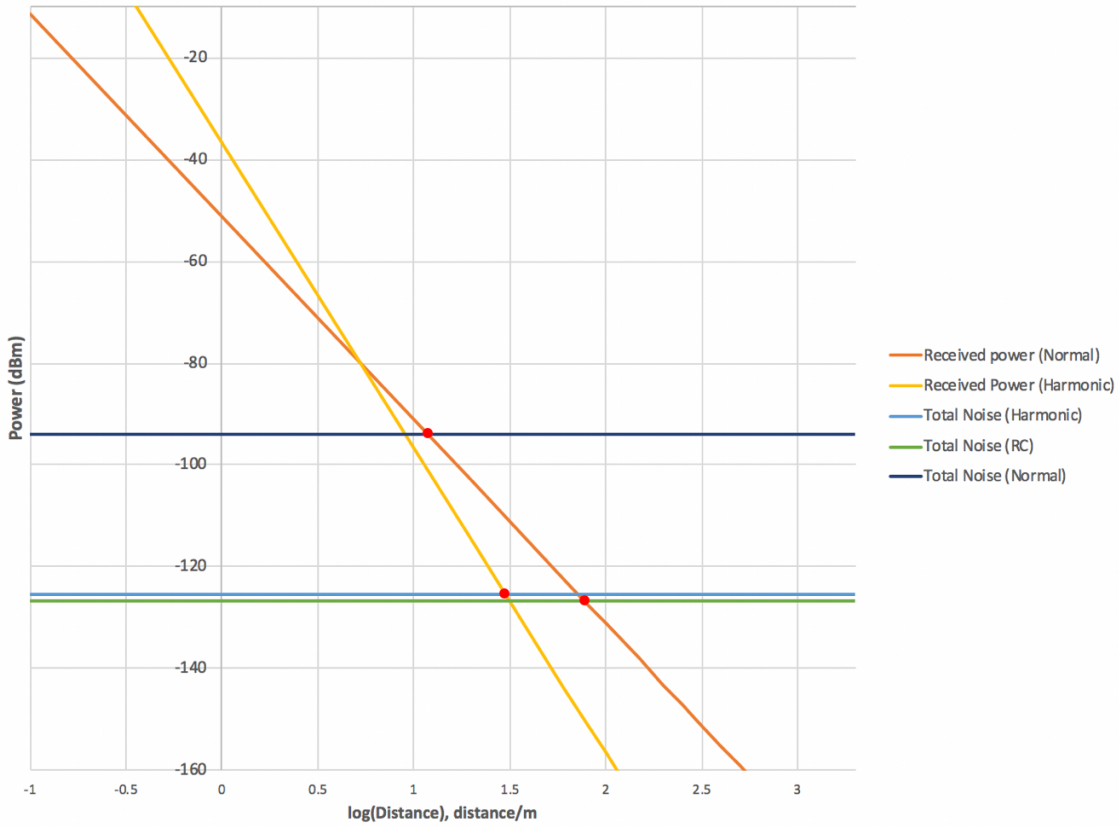


Figure 8. Plots of Received Power against  $\log(\text{Range})$  and Noise floors for the three models

It can be seen that the noise level brought down by RCE is very close to thermal noise, and in the case of our model even slightly lower than the thermal noise level. This illustrates that theoretically, RCE is very good at lowering the phase noise level. In reality, the phase noise reduction by RCE may not be as significant if time delays may be longer.

The ranges achieved of the 3 models are visualized by the 3 points marked in red in figure 8. It is observed that RCE produces the best result, giving the maximum range of 68m, with received power of -127dBm. The harmonic model achieves a communication range of 31m with received power of -125dBm. The normal model achieves a communication range of 13m with received power of -92dBm. The two models outperform the normal model in range by a significant difference, although lowering the received power by roughly 30dBm.

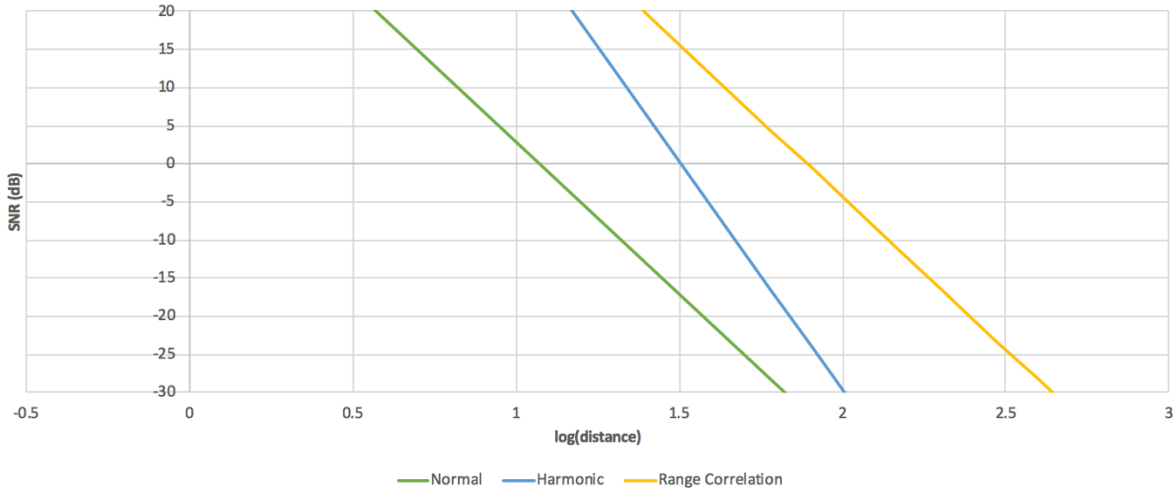


Figure 9. Plots of Received SNR against  $\log(\text{Range})$  of three models

Assuming the same modulation is used for all three systems, the three models will require the same minimum SNR for demodulation. For an SNR typically around 6dB, the plot in Figure 9 shows that RCE performs best, then the Harmonic, and the normal model performs worst. Therefore, the theory that RCE and using a harmonic backscatter tag improves the communication by a significant distance is validated.

## 4. Exploration of Better Coding Schemes

### 4.1 Motivation

In the project, it is wished to simulate more advanced coding schemes used by backscatter in order to improve the communication range.

As described in **Section 2.5** and **Section 2.8**, it is known that spread spectrum modulation techniques use a wide allocated bandwidth to broadcast a signal, making it the coding techniques resistive to channel noise and other interference [29]. Spread-Spectrum techniques have not yet been widely applied to backscatter except for [1] which presents a Lora-compatible backscatter design. We present two backscatter designs which use CSS and DS-SS (pseudo random binary coding) modulation techniques.

Moreover, exploiting Backscatter has the potential to simplify the system architecture compared to conventional DS-SS or CSS radio communication systems, and to lower the power consumption. As multiple bits are encoded per symbol at a bit rate is much higher than the rate of the symbol, timing is very important in Spread Spectrum techniques. Therefore, a stable high frequency LO is often required, increasing the power consumption. However, if the modulation process is can be replicated with backscatter, the power consumption of encoding will be much lower.

The performances of the CSS and DS-SS backscatter systems were compared using a MATLAB simulation. Moreover, as the presence of higher order harmonics in the modulated data is considered as the main limiting factor for performance, we also investigate the effect of removing the harmonics for the two coding schemes. The performances are evaluated by finding the achievable minimum SNR at a BER threshold of  $10^{-3}$  for all simulations.

## 4.2 System Model

### 4.2.1 System Model and Assumptions

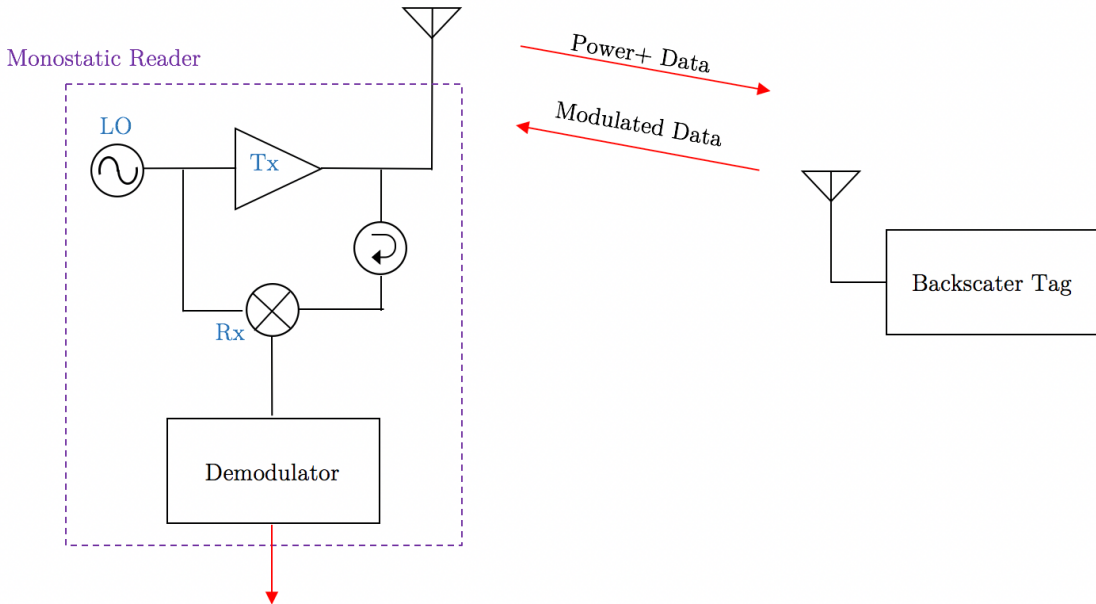


Figure 10. Backscatter System Deployment for Exploring Different Coding Schemes

A monostatic backscatter system is assumed for our simulations as shown in figure 10. Monostatic Backscatter holds the advantage against other radio systems of avoiding the problem of phase-difference, as it can use the same reference oscillator for transmitter and receiver. As the distance between the reader and tag is varied, the phase relationship between the backscattered signal and the LO into the receiver mixer will change. A distance can be reached when the two signals are  $90^\circ$  out of phase such that when the two signals are mixed before demodulating, zero phase can be achieved. Or, by IQ mixing when the phase of one of the signals is known, the phase of the second signal can be found out. Therefore, the frequency adjustment step that is added in typical radio systems may be avoided.

At the backscatter tag, a mixer performs the multiplication of RF signal and local oscillator, multiplying the carrier wave and the square wave switching between states produced by the backscatter RF switch. For our simulation, an equivalent baseband model was used to save computational memory and run time. Instead of simulating at

passband, where details of the RF carrier has to be simulated, only the backscatter-switched square wave is modelled, suppressing the RF carrier. Therefore, the number of sampling instants could be vastly reduced, consuming less memory and time, by allowing the simulation to be run around zero-frequency instead of at the RF carrier frequency.

The LO direct leakage at carrier frequency from Tx to Rx as illustrated in the reader structure in figure 10 will be ignored for simplification of simulation. Further, the model was simulated to only encode and decode one symbol at a time.

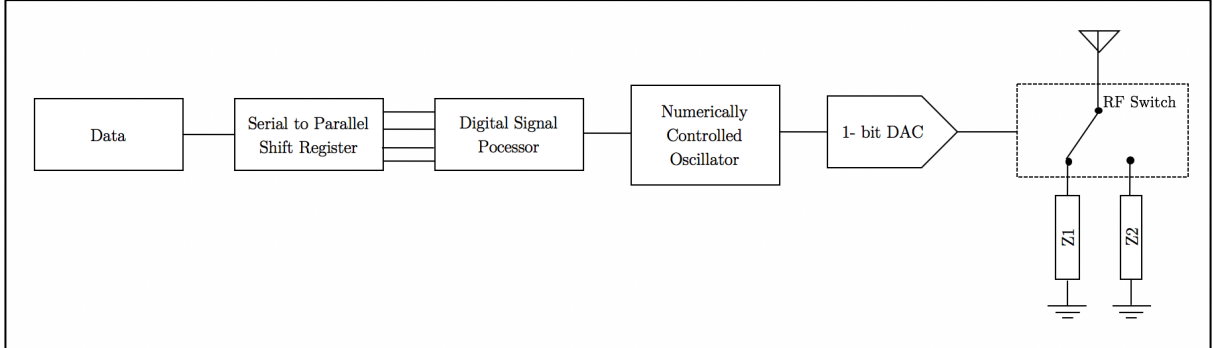


Figure 11. Simplified CSS Backscatter Tag Design Used for Simulation

The Backscatter Tag design illustrated in figure 11 was inspired by the Hybrid analog-digital Lora Backscatter design proposed in paper [1]. In the Lora backscatter device design presented in [1], the DSP produces the variable frequency square wave, and the DAC-VCO drives the antenna to switch between the impedances. A further simplification is done in our model by combining the DSP, DAC and VCO.

In our presented Backscatter design for CSS modulation shown in figure 11, the serial to parallel shift register allows encoding for multiple bits per symbol. The DSP process translates the bit stream information data into series of modulated increasing frequency waveform. This is then fed into a numerically controlled oscillator (NCO), such that the DAC only needs to be 1 bit to drive the switch with 2 impedance states. With the 1-bit DAC and the simple switch, the chirp can be produced digitally, which is the lowest power method of modulating the symbol.

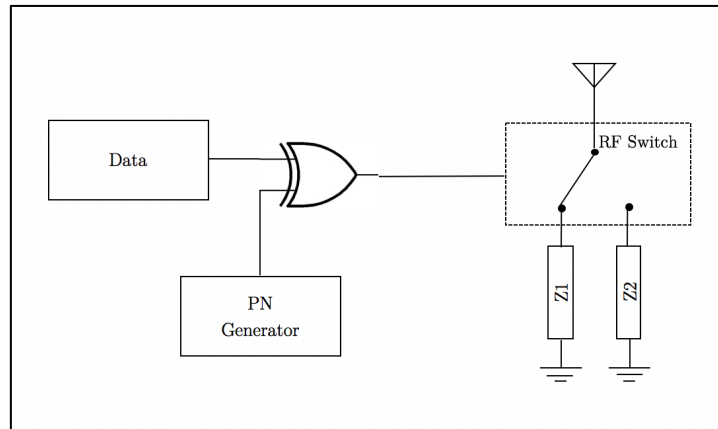


Figure 12. Simplified DS-SS Backscatter Tag Design Used for Simulation

Figure 12 shows the backscatter tag design for simulating the DS-SS modulation. The data received from the Tx is mixed with a unique pseudo-random binary sequence which modulates each data symbol. The random binary sequence is generated by a Pseudo-random noise generator (PRNG) at a much higher bit rate than the rate of the data. These are passed through an XOR gate to be mixed, and this is used to drive the binary backscatter switch. In DS-SS, the multiplication of data bits with a pseudo-random sequence which is at a higher frequency than actual data signal will result in a higher bandwidth. The resulting signal is expected to resemble white noise.

Although this project only explores the encoding of two schemes, theoretically, the a similar tag architecture with a backscatter switch as figure 11 and figure 12 could produce any other kind of binary coding scheme.

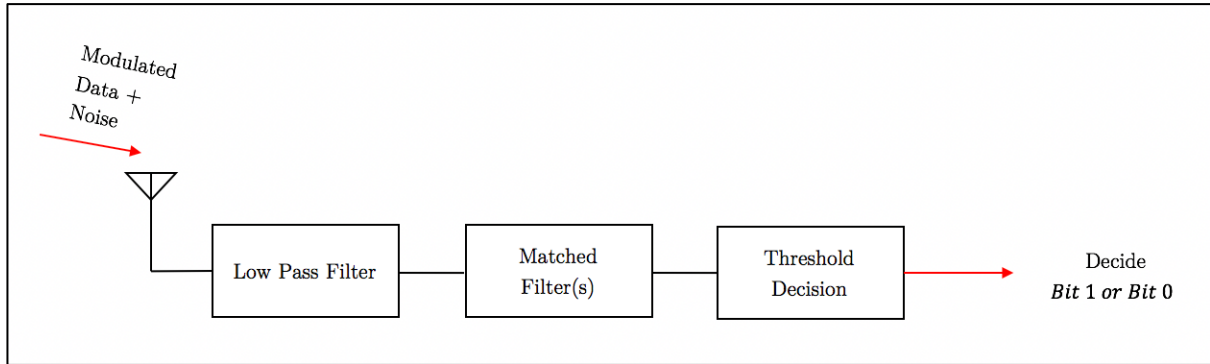


Figure 13. Generalized Receiver Structure used for Simulation

Figure 13 illustrates the receiver structure used in the simulation. The modulated data with noise from the AGWN channel is low pass filtered, then match-filtered to decode the symbol transmitted. In the simulation, noise was modelled as random white gaussian noise, and investigation was carried out to determine how much noise could be added to the signal for a bit error rate of  $10^{-3}$  to be achieved. The entire simulation was built using MATLAB from scratch, using only the communications toolbox for filter design and modelling the awgn channel.

The parameter assumptions made in simulation are shown in Table 2 below. These parameters are taken from a LoRa Simulation in [1].

|                  |             |
|------------------|-------------|
| Bandwidth        | 250 kHz     |
| Frequency Offset | 3 MHz       |
| Symbol Duration  | 100 $\mu$ s |

Table 2. Table of Parameter Assumptions for Simulation in **Section 4**

#### 4.2.2 Harmonic Content and Filtering

The backscatter SPDT switch with load tuners used in the design either reflects or absorbs the incident RF signals, creating square waves. The system is reliant on the switch switching between the two load tuners very quickly, up to 3.25MHz in the case of our simulation. One of the issues that arises is that this rapid instantaneous switching causes power leakage into the third and fifth harmonics in adjacent frequency bands, resulting in interference and degrading performance. An increase in bit error probability is expected in the presence of harmonics in data as it adds noise, increasing the difficulty of decoding.

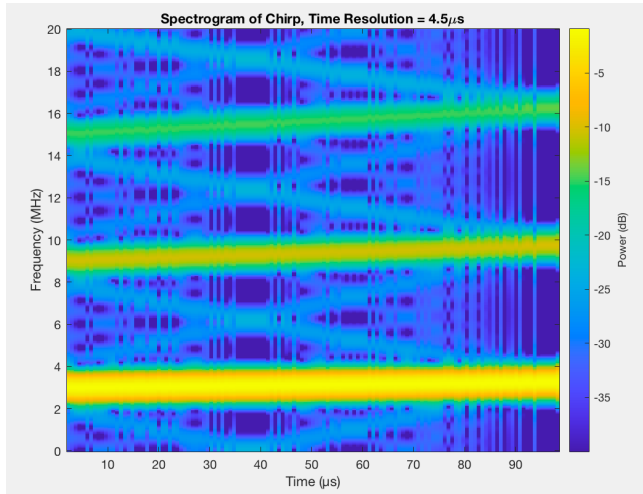


Figure 14. Spectrogram of perfect linearly-increasing Chirp, Containing Harmonics

The two steeper lines at higher frequencies in figure 14 illustrate the presence of harmonics in the perfectly coded chirp symbol with incorporated no delay in switching. Although the higher order harmonics are at lower power levels than the main chirp, the power leakage of the 3<sup>rd</sup> harmonic at around -10dB is considered significant. The vertical artefacts seen in the spectrogram can be disregarded as they are thought to be MATLAB artefacts in spectrogram plotting.

In reality, the perfect instantaneous switching is limited by the rise time of the backscatter SPDT switch. The delay of each switching is incorporated into the simulation as a first low pass filter illustrated below in figure 15. The '1<sup>st</sup> LPF' was inserted to emulate the realistic delay in switching between two states of the switch and this filter was implemented for all simulations.

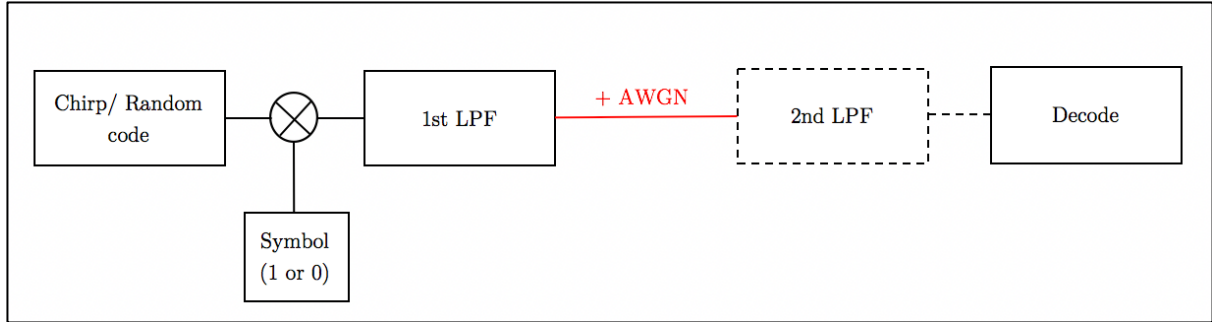


Figure 15. Block diagram of Simulation Progression, illustrating the use of the two LPFs

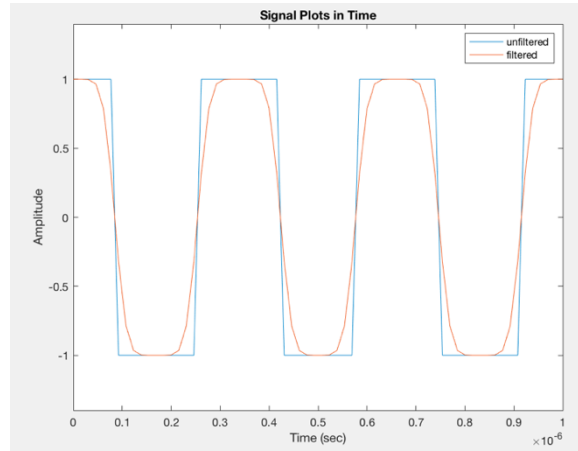


Figure 16. Plot comparison of Filtered and Unfiltered signals in time, illustrating the Delay in Switching

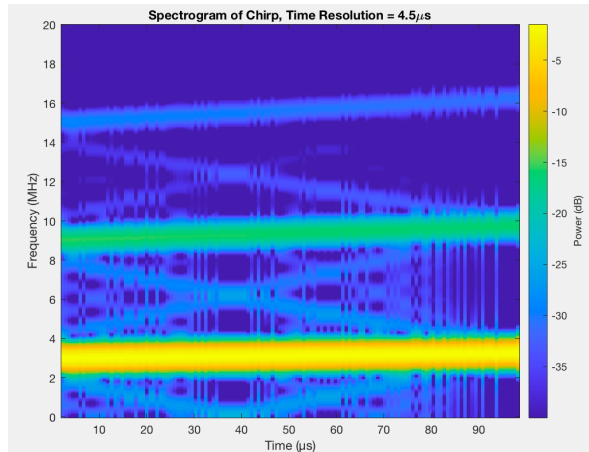


Figure 17. Spectrogram of Linear Chirp after the 1<sup>st</sup> LPF that removes sharp transitions in switching

As seen in figure 16, the power leakage in the higher order frequency bands are still prominent after incorporating the switching delay in backscatter. Therefore, it was decided that a 2<sup>nd</sup> LPF with a higher filter order would be applied if we wished to completely suppress this leakage. In terms of the simulation architecture, after the 1<sup>st</sup>

LPF which was applied to all simulations, the 2<sup>nd</sup> LPF was applied optionally depending on whether we wished to include or remove the higher order harmonics in the data in each simulation. The effect of the optional 2<sup>nd</sup> LPF which completely suppresses higher order harmonics is illustrated figure 19.

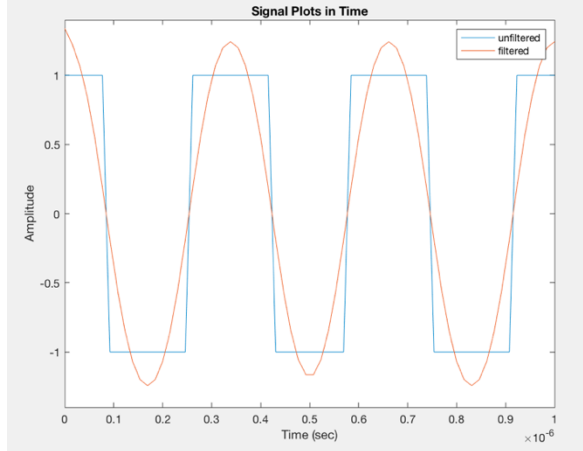


Figure 18. Plot of Harmonics-removed signal after the 2<sup>nd</sup> LPF, and Unfiltered signal in time

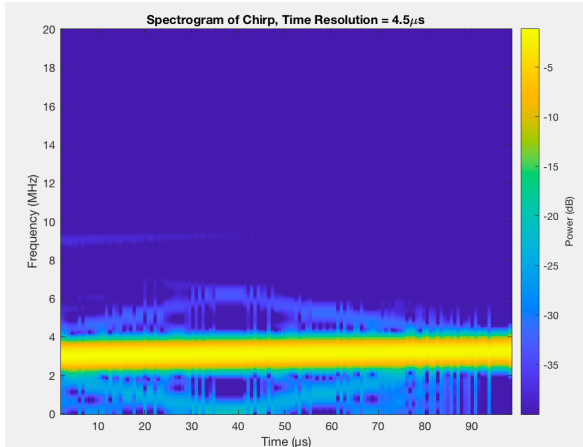


Figure 19. Spectrogram of Linear Chirp after the 2<sup>nd</sup> LPF suppressing harmonics

From figure 19, it can be observed that the 3<sup>rd</sup> and 5<sup>th</sup> harmonics are almost completely suppressed by the second filtering operation.

Theoretically, although filtering out higher order harmonics is expected to lower interference and improve performance [1], some of the useful power is being abandoned by the low-pass filtering operation. Therefore, investigation will be carried out to find out whether the improved correlation properties of removing higher order harmonics overpowers the effect of abandoning useful power in the harmonics by filtering.

To summarize, the following investigations aims are to be achieved for the rest of **Section 4**:

1. Comparing the performances of Random Binary Coding and CSS modulation

2. Comparing the performances for when harmonics are present/absent in the modulated signal for both coding schemes, decoded with its optimal matched filter in each case
3. Validate that the optimal matched filter design for each case is obtained using the input to the matched filter as described in **Section 2.7**

For all investigations, the performance evaluation is conducted by comparing the minimum SNR achieved at a bit error rate of  $10^{-3}$ .

### 4.3 CSS Backscatter

In slope-shift keying, which is the simplest type of CSS, the up-chirp is defined as symbol ‘1’ and a basic down-chirp is defined as symbol ‘0’ as illustrated below.

#### 4.3.1 CSS Encoding

##### Up-Chirp (Symbol 1)

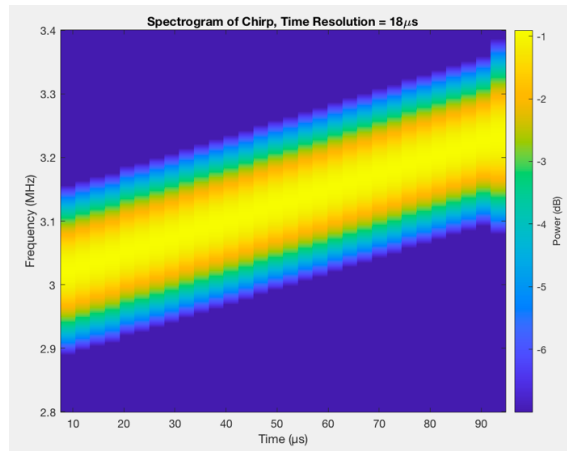


Figure 20. Spectrogram of Up-chirp in the fundamental frequency range

Using the parameter assumptions in Table 2, the up-chirp symbol increases from offset of 3MHz to 3.25MHz with a 250kHz bandwidth within the symbol duration of  $100 \mu s$ . Figure 20 shows a zoomed-in spectrogram of the chirp created using our backscatter tag design.

##### Down Chirp (Symbol 0)

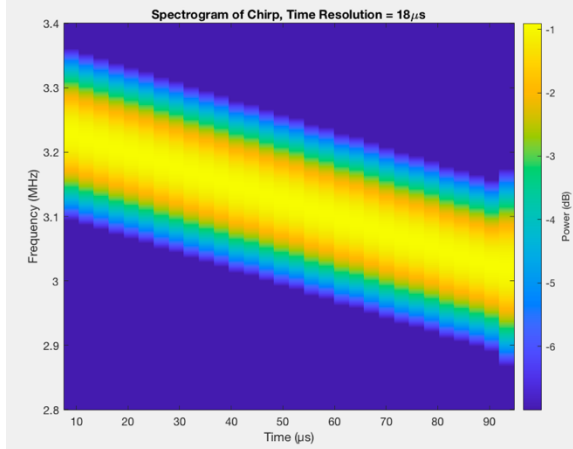


Figure 21. Spectrogram of Down-Chirp in the fundamental frequency range.

Similarly, as seen in figure 21, the down-chirp symbol decreases from 3.25MHz to 3MHz with a 250kHz bandwidth within the symbol duration of 100  $\mu\text{s}$ .

#### 4.3.2 CSS Decoding

The transmission of the coded symbol via an AWGN channel is modelled by adding random seed gaussian noise to the encoded symbol with a specified SNR. The MATLAB *awgn* function was used to model the channel noise.

$$P_{noise} = \frac{P_{signal}}{SNR_{specified}} \quad (7)$$

The *awgn* function measures the input signal power to incorporate it with the desired SNR level specified to produce a an output signal with the gaussian noise level added. SNR levels were varied to vary the levels of noise added to the signal, as illustrated in figure 22 below.

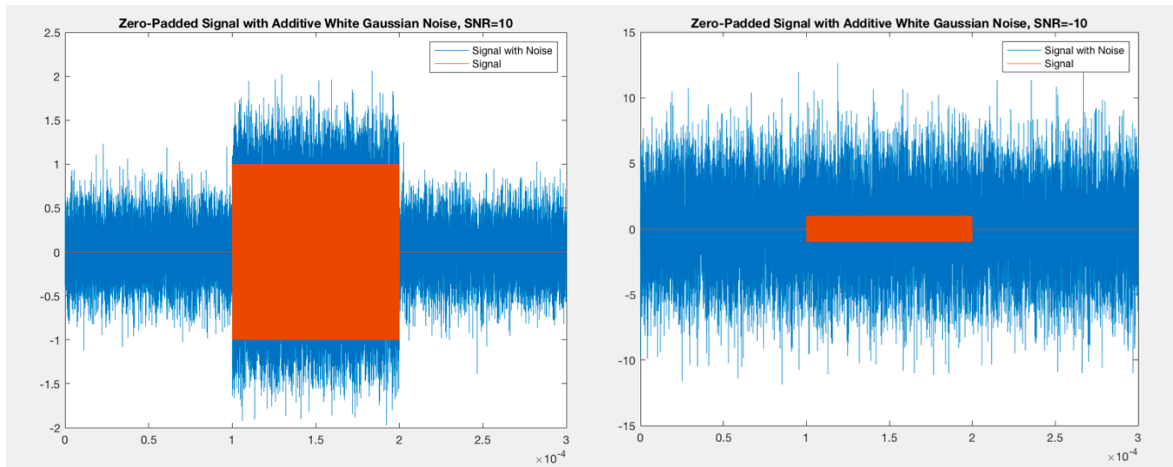


Figure 22. Zero-padded CSS-modulated symbol with AWGN in time,  
SNR= -10 (left) and SNR= 10 (right)

Figure 22 shows a single symbol at the receiver input with different amounts of added noise varied using SNR values. The symbol transmitted was zero padded on both sides for easier visualization of the matched filtered output of signal after decoding.

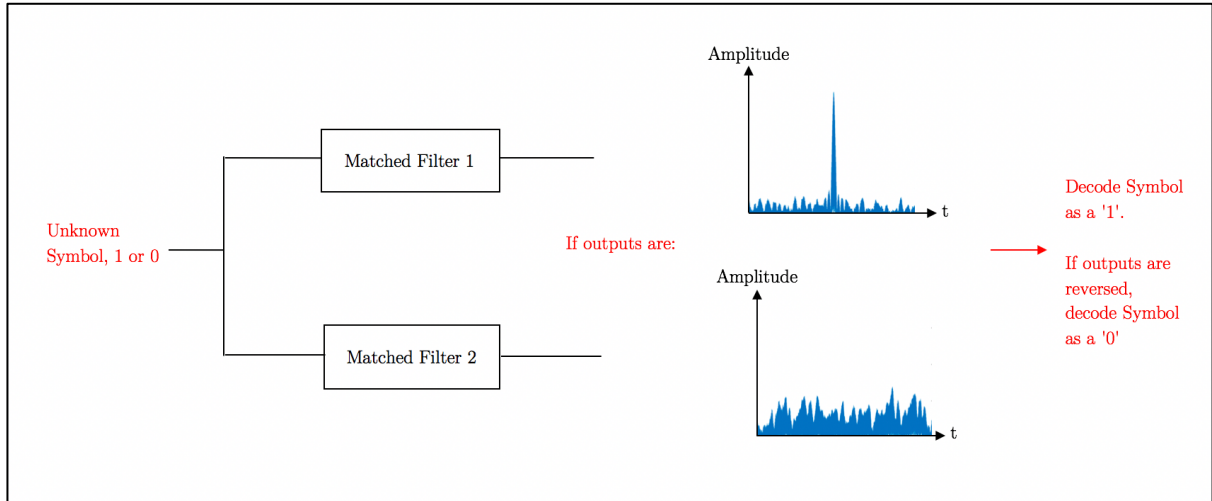


Figure 23. Block diagram Illustration of CSS Decoding

Figure 23 shows our system logic for decoding a chirp symbol. An unknown symbol with added noise is passed through two matched filters. The coefficients of two matched filters are obtained by taking the conjugate of time-reversed version of the up and down chirp signals respectively. In figure 23, the coefficients of ‘Matched Filter 1’ are designed to be the conjugate of the time-reversed copy of Symbol 1, and the coefficients of ‘Matched Filter 2’ are the conjugate of the time-reversed copy of Symbol 0. The match-filtered outputs shown on the right are the convolution of the unknown signal with the corresponding matched filter coefficients. The absolute values of the decoder outputs were used for detection.

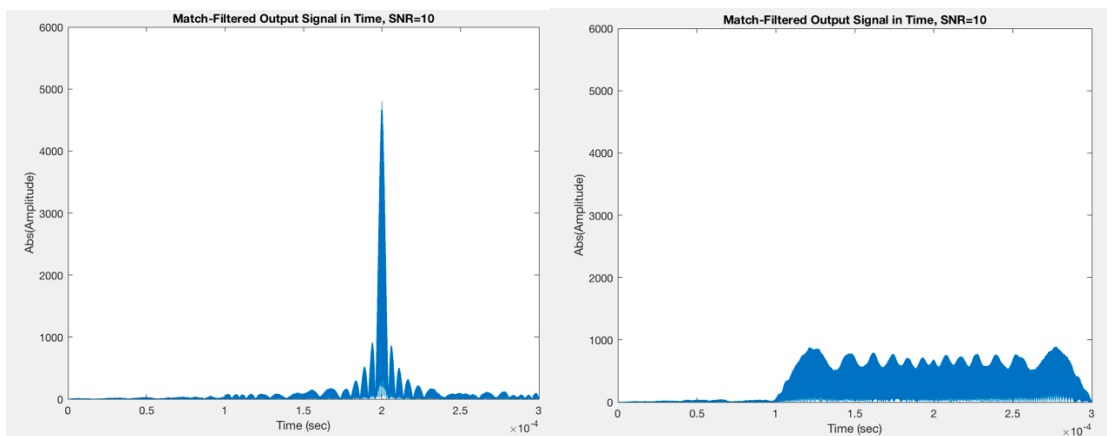


Figure 24. Outputs from the two Matched-filters, SNR=10

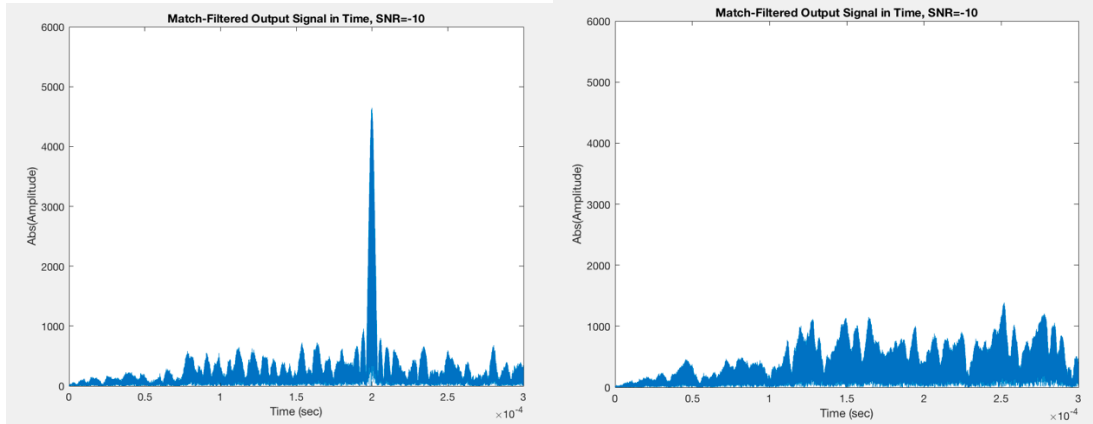


Figure 25. Outputs from the Two Matched-Filters,  $\text{SNR} = -10$

Figures 24 and 25 illustrate the increasing difficulty of detection of the correct symbol as SNR decreases. At some negative SNR value low enough, the noise level will be too high such that the correlation peak will be indistinguishable from the noise.

The observed correlation peak is relatively wide with significantly wide sidebands. A better coding scheme is expected to give a matched filtered peak such that more of the energy in the ripples are incorporated into the main peak, increasing the system's robustness to noise.

#### 4.3.3 BER vs SNR Simulation

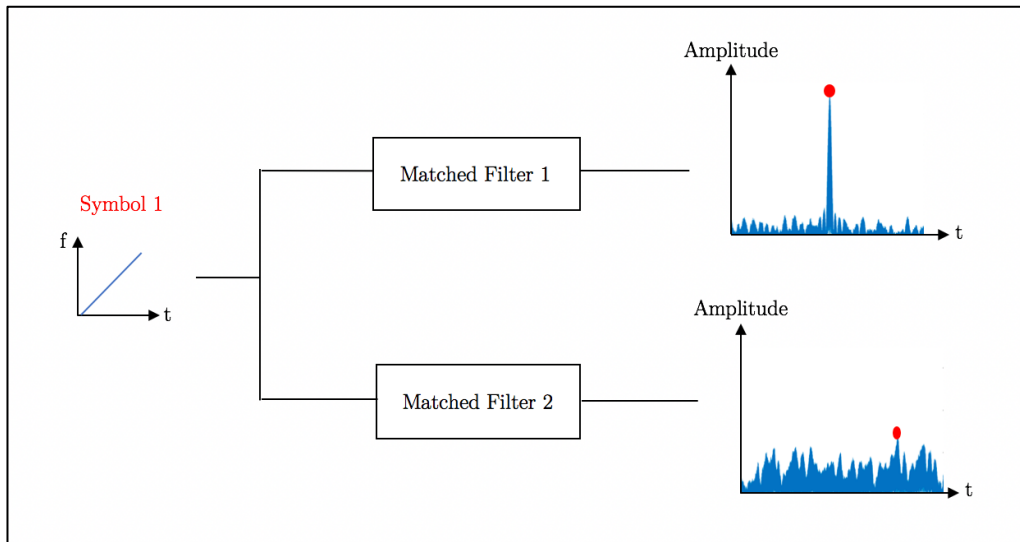


Figure 26. Block Diagram Illustration of Error Detection for CSS-Decoding

Figure 26 illustrates the simulation logic for error detection of a chirp symbol. This exact logic was used to calculate the bit error probability for a certain SNR specified. Symbol 1 (Up-chirp) is fed into two matched filters, and only one of the outputs to the filters would produce a correlation peak. Noise was added by a specified SNR until errors

occurred. The error was defined to be when the maximum amplitude of the output to ‘Matched Filter 2’ was greater than the maximum amplitude of the output of ‘Matched Filter 1’, as shown by the red dots in figure 26.

50,000 simulations were carried out for each specified value of SNR, to produce the SNR vs BER plots below. Figures 27 to 29 show the zoomed-in SNR vs BER plots used to obtain the minimum SNR values for a bit error rate crossing of  $10^{-3}$ , and the result is summarized in Table 3.

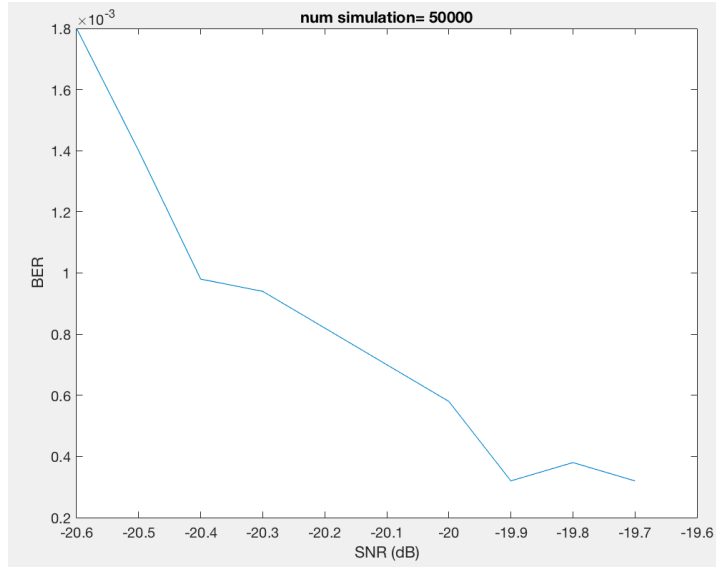


Figure 27. Plot of SNR vs BER of Harmonics-removed Chirp through a Harmonics-removed Matched Filter

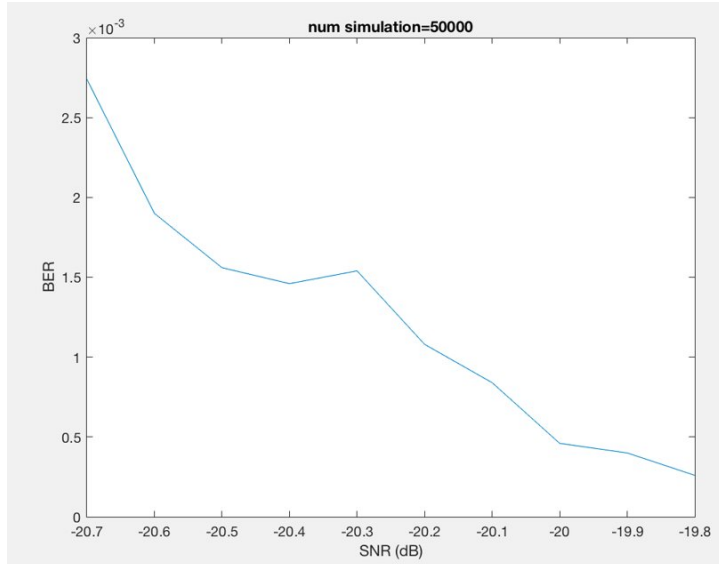


Figure 28. Plot of SNR vs BER of Harmonics-included Chirp through a Harmonics-included Matched Filter

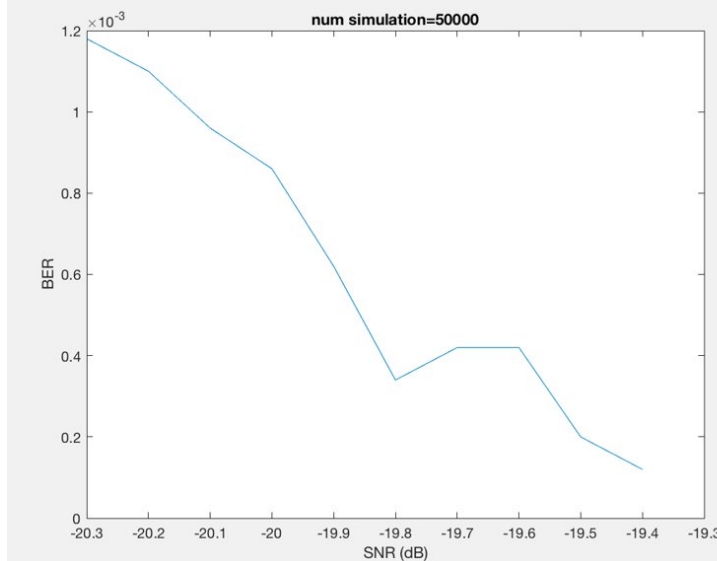


Figure 29. Plot of SNR vs BER of Harmonics-included Chirp through a Harmonics-removed Matched Filter

| Simulation Type                                   | Min SNR achieved at BER = $10^{-3}$ |
|---|-------------------------------------|
| Harmonics-included CSS with harmonics-included MF | -20.2                               |
| Harmonics-removed CSS with harmonics-removed MF   | -20.4                               |
| Harmonics-included CSS with harmonics-removed MF  | -20.1                               |

Table 3. Table of Results for Chirp Simulation

Comparing the first two results obtained in Table 3, the SNR achieved by a harmonics-removed signal is better than the SNR achieved by the harmonics-included signal. Therefore, it can be concluded that for chirp modulation, removing the harmonics in the signal minimizes interference to give a lower bit error rate, improving the communication range achievable by backscatter. This validates the theory that the effect of filtering to minimize interference overpowers the effect of neglecting significant amounts of power present in the higher order harmonics.

Moreover, comparing the last two results of Table 3, it can be concluded that the optimal matched filter for the harmonics-included signal is the matched filter designed with coefficients produced by a signal with its harmonic content removed.

However, the difference between the SNR values obtained are very small. Therefore, overall it can be concluded that for the simple Slope-shift-Keying CSS modulation, the presence of higher order harmonics by backscatter doesn't realistically affect the performance.

In the scope of our experiment, we have only considered one user communicating over the channel. In realistic CSS applications, harmonics in the signal is also a major issue in multi-user interference, which will be described in more detail in **Section 7**.

#### 4.3.4 FSCSS Backscatter

The proposed LoRa backscatter design in [1] is one of the very few schemes proposed which exploits backscatter to achieve long-range communication for wireless technology. LoRa uses the FSCSS modulation technique, where the bits encoded are linearly increasing frequency chirps and their cyclic shifts. In FSCSS, the spreading factor (SF) determines the length of the spreading code (chirp), and provides a tradeoff between data rate and range [30]. Choosing a higher spreading factor can increase the range but this will decrease the data rate and vice versa. In FSCSS, each symbol is spread by a modulating code of length  $2^{SF}$  bits. So, for SF=1, two options of coding are available, and for SF=2, 4 options of coding are available, depending on the amount of cyclic shifting of the chirp. LoRa typically employs SF between 7 to 12.

In this section, FSCSS encoding and decoding was attempted with SF=1 and SF=2 as a kickstart to investigate if this coding scheme could be applied to our model.

##### SF=1

When SF=1, the coding scheme can encode 2 symbols. An unshifted basic linear chirp as in figure 20 would be Symbol 1, and Symbol 0 would be a half-cycle shifted version of the linear chirp is as shown in figure 30 below.

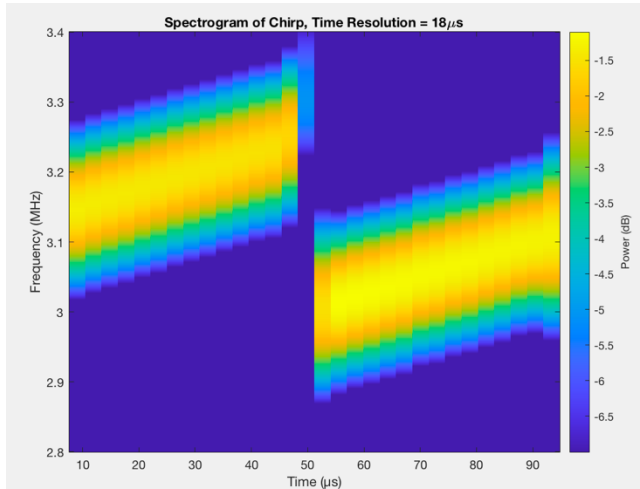


Figure 30. Spectrogram of the Shifted Symbol (Symbol 0) Encoded by FSCSS modulation with SF=1

This symbol was attempted to be decoded using two matched filters and locating a correlation peak. The coefficients of the two matched filters are designed to be conjugate time-reversed versions of the two symbols defined above.

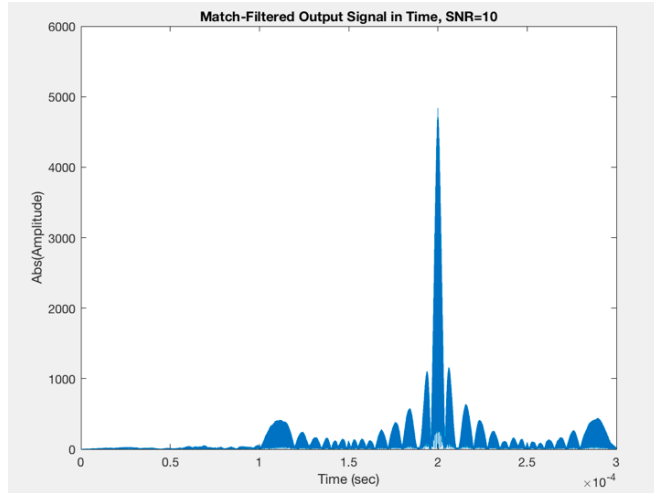


Figure 31. Match-filtered Output when a Shifted Signal (Symbol 0) is fed into a MF with coefficients created from Symbol 0

Figure 31 shows the output of the shifted signal to a matched filter with coefficients produced from the same shifted signal. In this case, the peak can be located without much difficulty.

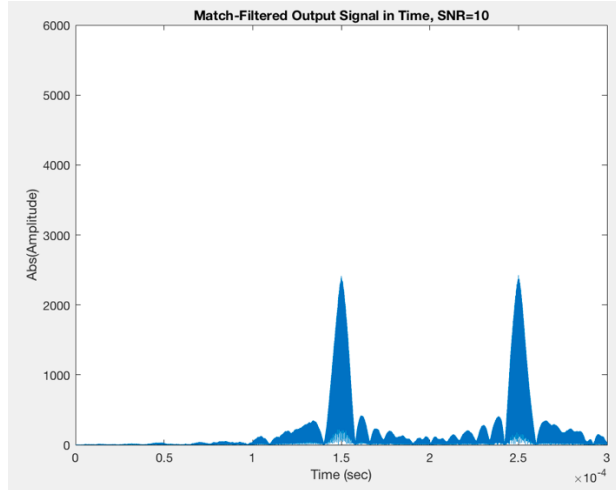


Figure 32. Match-filtered Output when a Shifted Signal (Symbol 0) is fed into a MF with coefficients created from Symbol 1

However, when the shifted signal is fed into a matched filter made up of coefficients produced from the other unshifted symbol, the output produces two peaks separated by the symbol duration. The problem arises as the second peak is shifted outside the duration of the symbol, and as multiple symbols are sent over the channel, this will cause interference, increasing the difficulty of decoding.

### SF=2

Similar results appear when SF=2 and the scheme can encode four different symbols. The spectrogram of one of the four symbols is shown below in figure 33 for visualization.

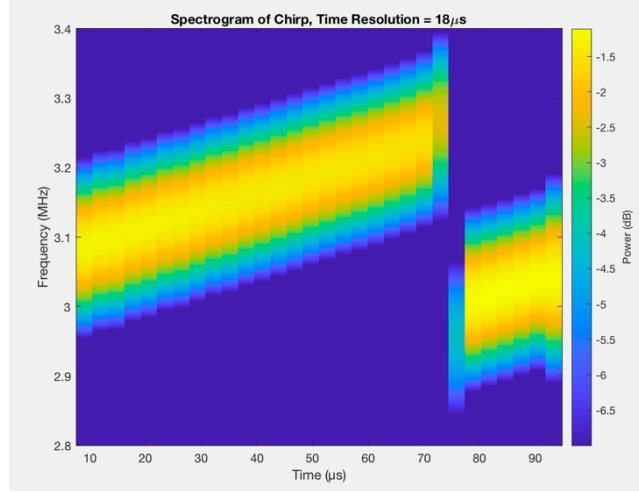


Figure 33. Spectrogram of One of the Shifted Symbols Encoded by FSCSS Modulation with SF=2

In this case, to be compatible with our decoding architecture, four matched filters would have to be implemented, each with coefficients produced from the 4 cyclically shifted symbols.

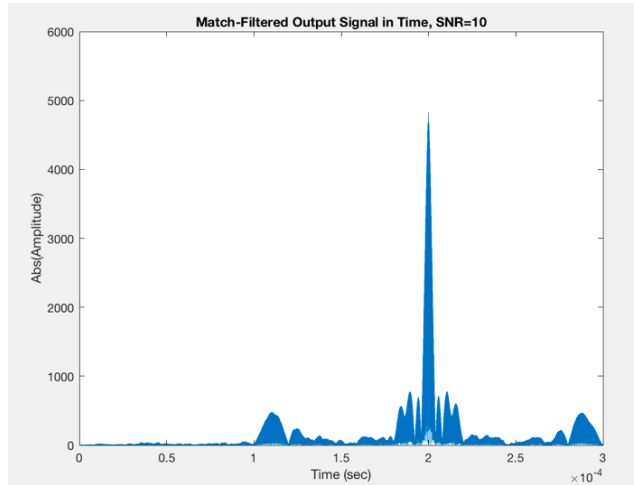


Figure 34. Match-filtered Output when a Quarter-Shifted Symbol is fed into a MF with Coefficients created from Quarter-Shifted Symbol

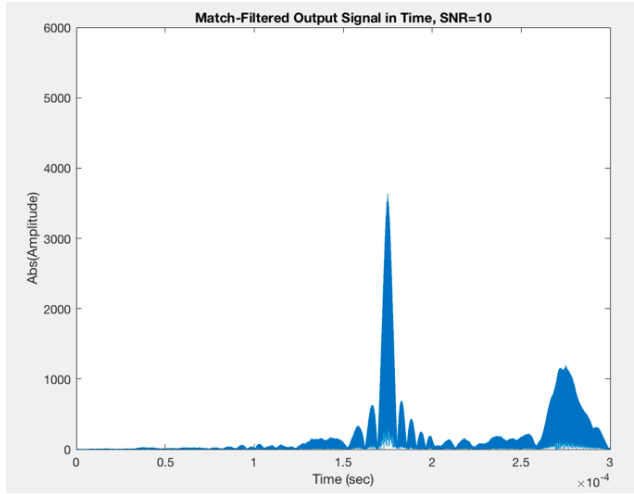


Figure 35. Match-filtered Output when a Quarter-Shifted Symbol is fed into a MF with Coefficients created from Unshifted Symbol

Similarly to when SF=1, Although symbols can be decoded without much difficulty for one of the four encoding schemes as shown in figure 34, the other three coding schemes cause a problem in decoding. As it can be seen in figure 35, the second peak is located outside the symbol duration, expecting to cause interference and if multiple symbols are sent. Further, with our system structure, this coding scheme would require different matched filters to be used for different cyclic shifts in the context of our model, increasing undesired complexity.

Therefore, it was decided to withhold the investigation, and further investigation to resolve this issue was left for future work.

## 4.4 DS-SS Backscatter (Random Binary Sequence Coding)

### 4.4.1 DS-SS encoding

MATLAB's *randi* function was used to replicate the random bit generation done at the PN generator. To enable comparison between the DS-SS and CSS backscatter, the random binary symbols were created by sampling at the highest frequency of the chirp which is 3.25MHz. For our symbol duration of  $100 \mu\text{s}$ , 325 random bits were used to create Symbol 1, and Symbol 0 was created by simply reversing each of the 325 bits, as visualized in figure 36 below.

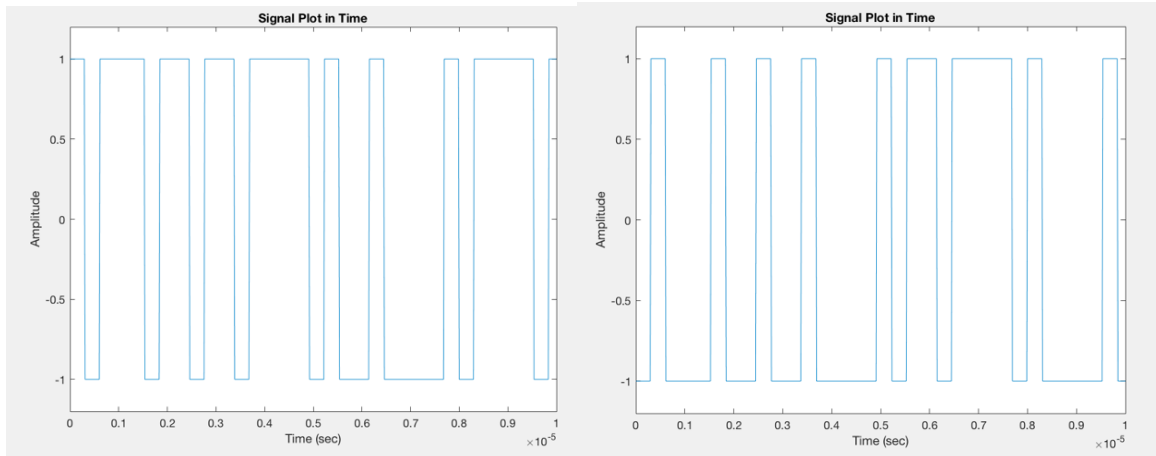


Figure 36. Zoomed-in Signal Plot of Symbol 1 (left) and Symbol 0 (right) in time

Figure 36 shows zoomed-in plots of the unfiltered DS-SS modulated symbols. Then, all random-binary signals, as with the chirp, were lowpass filtered remove sharp edges to incorporate the delay in switching.

#### 4.4.2 DS-SS Decoding

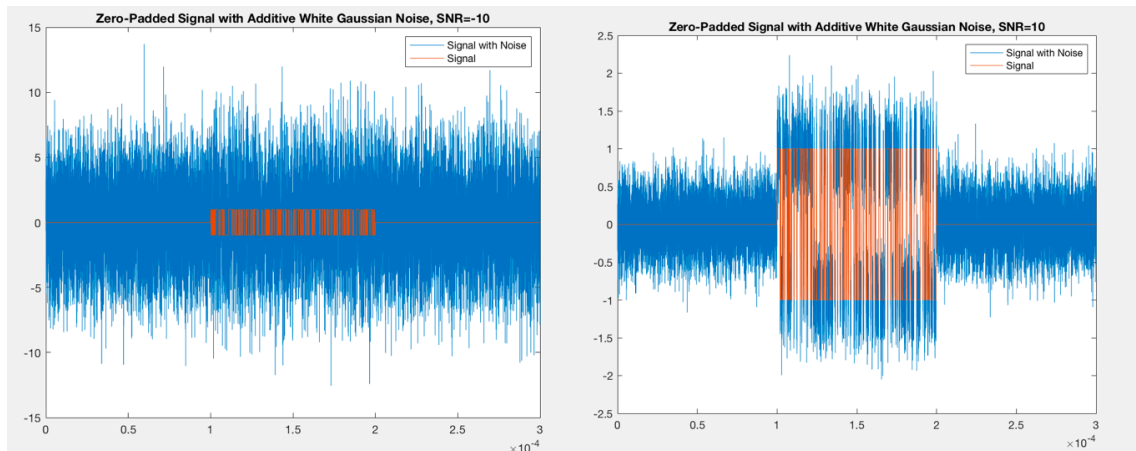


Figure 37. Zero-padded DS-SS modulated symbol with AWGN in time, SNR= -10 (left) and SNR= 10 (right)

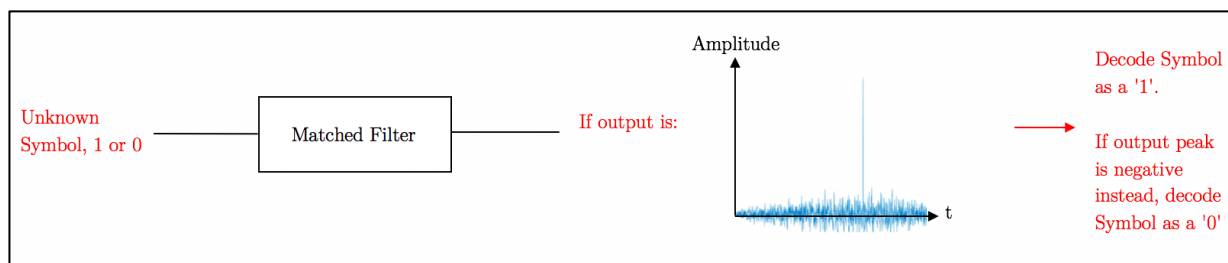


Figure 38. Block diagram Illustration for Decoding a DS-SS modulated symbol

Unlike the decoder design for CSS, the decoding process in DS-SS only requires one matched filter. As there is no pattern associated with the random encoding, the correlation peak detection can be done with a single one matched filter. If the matched filter coefficients are designed to be the conjugate time-reversed samples of ‘Symbol 1’ defined in encoding, feeding in a ‘Symbol 1’ will produce a positive peak, and ‘Symbol 0’ will produce a negative peak. Only the sign of the peak has to be observed to detect the signal correctly.

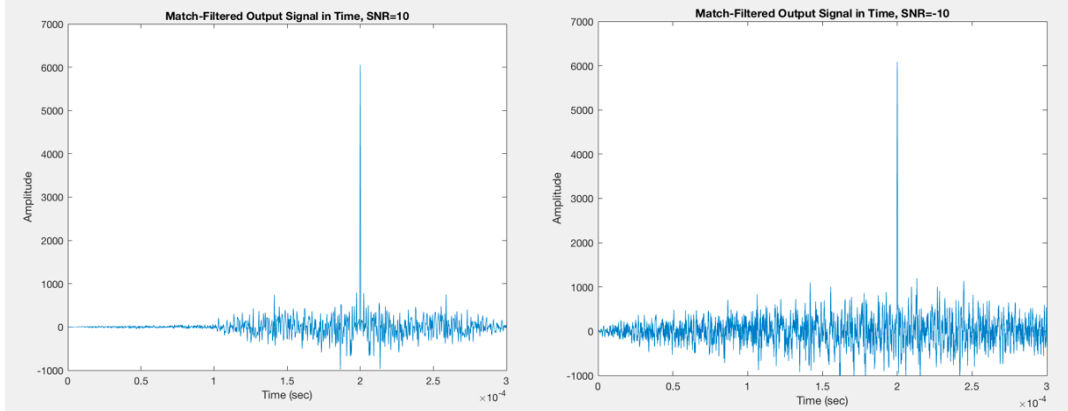


Figure 39. Match-filtered Outputs when Input Symbol is ‘1’,  
SNR=10 (left) and SNR=−10 (right)

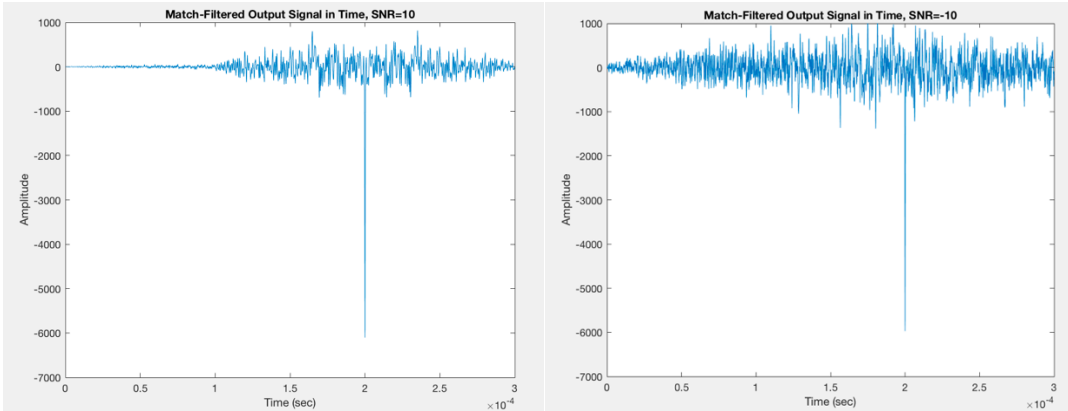


Figure 40. Match-filtered Outputs when the Input symbol is ‘0’,  
SNR=10 (left) and SNR=−10 (right)

It can be observed that the correlation peak produced by DS-SS backscatter is much sharper than for CSS, with much less significant sidebands. Further, the peak amplitude is greater for the DS-SS, illustrating that more energy is concentrated in the main peak, which makes the decoding process easier than CSS.

However, sometimes in detection, a correlation peak that is too narrow could cause problems. If the sample clock is out even by a small timing offset, due to a frequency offset between the Tx and Rx, the correlation peak could be missed. This requires clocks

to be needs to be perfectly aligned and to sample at the exact instants for decoding. Therefore, it is very important to oversample and have good receiver sensitivity.

#### 4.4.3 BER vs SNR Simulation

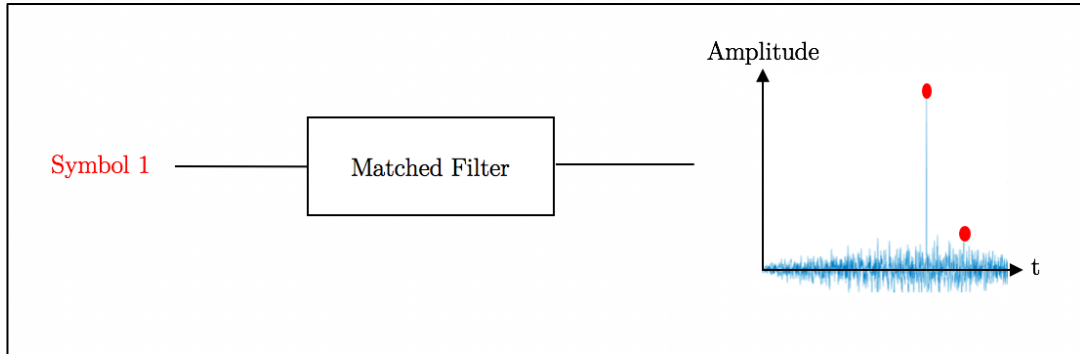


Figure 41. Block Diagram Illustration of Error Detection for DS-SS Decoding

Figure 41 shows the logic for error detection of a symbol encoded using a unique random binary sequence. ‘Symbol 1’ with added noise from the AWGN channel is fed through a matched filter designed using the same data without added noise, and the output produces a correlation peak. An error was detected if the correlation peak was buried in the noise, by comparing output amplitudes as illustrated by the red dots in figure 41. The error was defined to be when the maximum amplitude of the output was negative.

This exact logic was used to calculate the bit error probability for a certain SNR. 50,000 simulations were carried out for each specified value of SNR, to produce the SNR vs BER plots below. Figures 42 to 44 show the zoomed-in SNR vs BER plots used to obtain the minimum SNR values for a bit error rate crossing of  $10^{-3}$ , and the result is summarized in Table 4.

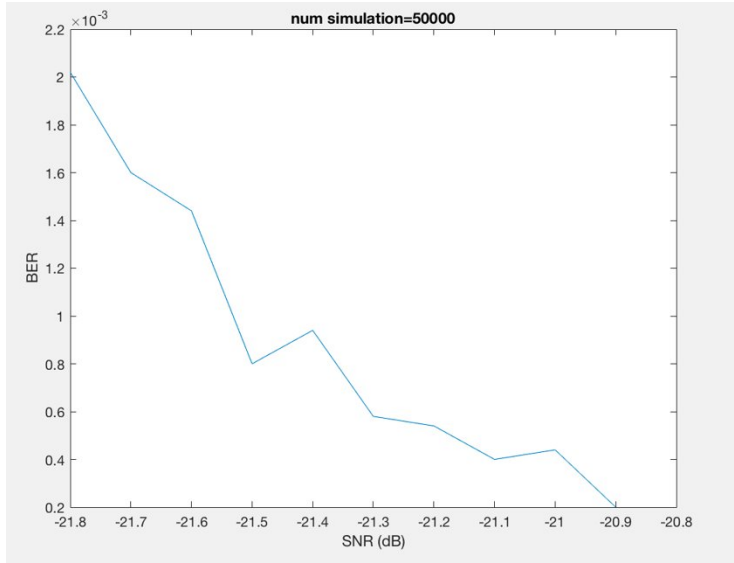


Figure 42. Plot of SNR vs BER of Harmonics-included DS-SS through a Harmonics-included Matched Filter

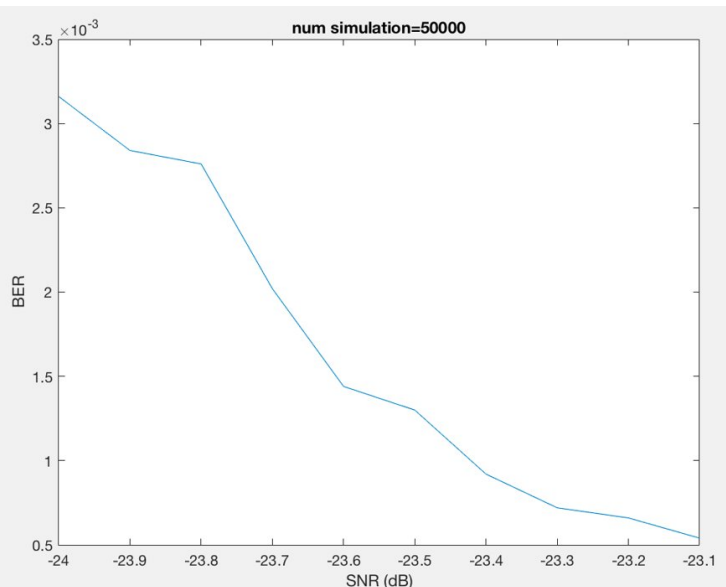


Figure 43. Plot of SNR vs BER of Harmonics-removed DS-SS through a Harmonics-removed Matched Filter

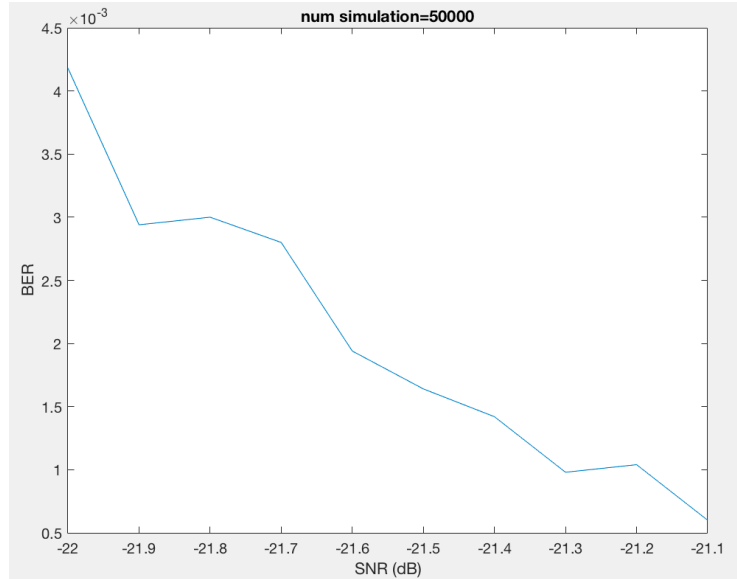


Figure 44. Plot of SNR vs BER of Harmonics-included DS-SS through a Harmonics-removed Matched Filter

| Simulation Type                                     | Min SNR achieved at $\text{BER} = 10^{-3}$ point |
|---|--|
| Harmonics-included DS-SS with harmonics-included MF | -21.5  |
| Harmonics-removed DS-SS with harmonics-removed MF   | -23.4  |
| Harmonics-included DS-SS with harmonics-removed MF  | -21.3  |

Table 4. Table of Results for DS-SS Backscatter Simulation

Comparing the top two results summarised in Table 4, it can be concluded that removing the harmonics in the signal for DS-SS improves performance quite significantly, lowering the minimum SNR required by almost 2dB. This again, concludes that the effect of filtering the harmonics in adjacent sidebands to reduce interference should be prioritised over the neglected power contained in the higher order harmonics.

#### 4.5. CSS vs DS-SS Discussion

To compare the results obtained from CSS and DS-SS Backscatter, a combined SNR vs BER plot was drawn.

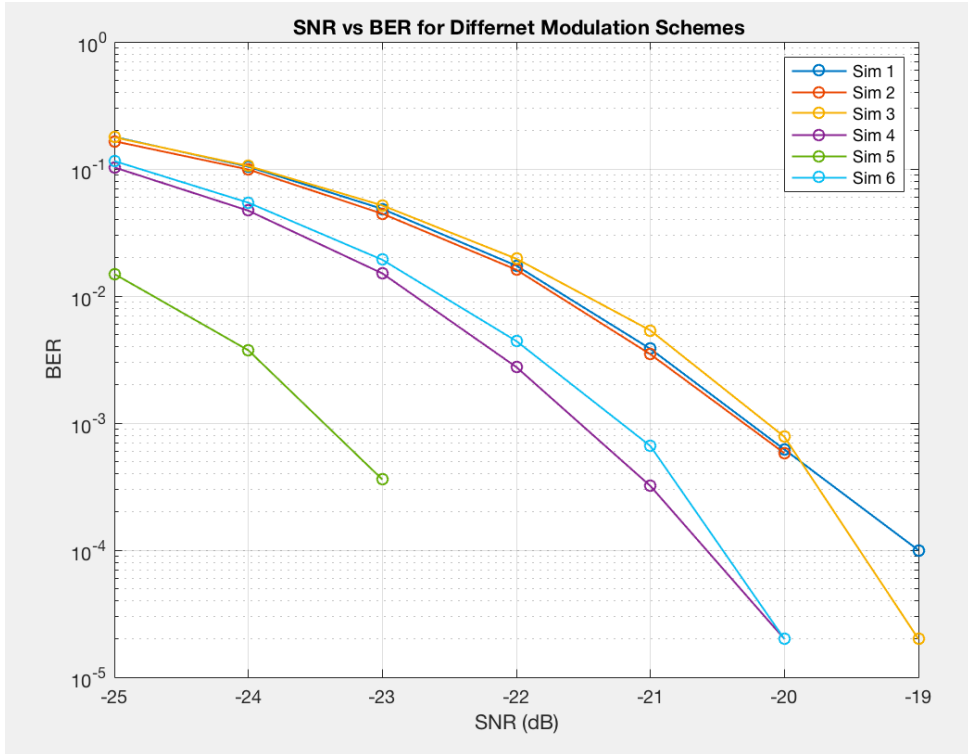


Figure 45. SNR per bit vs Symbol Error Rate plots for Different Schemes

| Key   | Simulation Type                                     |
|-------|---|
| Sim 1 | Harmonics-included CSS with harmonics-included MF   |
| Sim 2 | Harmonics-removed CSS with harmonics-removed MF     |
| Sim 3 | Harmonics-included CSS with harmonics-removed MF    |
| Sim 4 | Harmonics-included DS-SS with harmonics-included MF |
| Sim 5 | Harmonics-removed DS-SS with harmonics-removed MF   |
| Sim 6 | Harmonics-included DS-SS with harmonics-removed MF  |

Table 5. Table showing a key used in Figure 45 for different simulation types

The abrupt stop in Sim 5 in figure 45 can be interpreted as a zero bit error for the 50,000 simulations conducted. This is an achieved BER of much less than  $2 * 10^{-5}$  on average. Comparing the results of CSS (Sim 1-3) and DS-SS (Sim 4-6) backscatter, from figure 45, it can be seen that DS-SS coding outperforms CSS in all cases. DS-SS achieves a significantly lower minimum SNR for the same BER compared to CSS.

From table 5, comparing the optimal performances achieved in both coding schemes (Sim 2 & Sim 5), DS-SS achieves a minimum SNR of 3dB lower than CSS. Assuming the same power is transmitted, and assumptions on noise are equivalent, this means that half the amount of power is required at the receiver for the random coding model. This is equivalent to concluding that the combined two-way-path-loss in backscatter can be doubled for a DS-SS backscatter coding scheme compared to CSS. For a monostatic backscatter design, this is an increase in communication range of a factor of  $\sqrt[4]{2} = 1.19$ . This is a significant factor, and holds the potential to increase the

communication range by a significant difference in backscatter. Using the achievable range of a monostatic model with RCE obtained from the spreadsheet modeling, which is 68m given our assumptions, this is an increase of communication of 13m by using DS-SS compared to CSS.

Further, for both modulation schemes, it is seen that removing the higher order harmonics created by the rapid backscatter switching improves performance. Removing the harmonics improves the performance much more significantly for Random Binary coding, whereas for chirp encoding, the difference in performance was negligible. This shows resistance of CSS modulation to harmonic content in the data. Because backscatter systems will always suffer from the harmonic content created by the rapid switching, without a harmonic cancellation mechanism or a high order LPF at the receiver, this cannot be avoided. The robustness of CSS illustrates its potential, although its absolute performance is outperformed by DS-SS.

However, this result doesn't correlate with the assumptions used in other papers including [1] that CSS is particularly susceptible to harmonic content. This disparity was thought to have arisen because a simple 'slope shift keying' method was used in our project, failing to encapsulate the full process of CSS coding which is typically used. Further, in recent applications of CSS, almost always FSCSS is used instead. Moreover, only one symbol was transmitted in each simulation, disregarding the usual problems in CSS with symbol overlap and multi-user interference. Further investigations regarding this issue is left for future work. It is concluded that discovery that lowpass filtering largely improves performance for DS-SS almost by 2dB is a significant discovery in itself.

## 5. Proposed Long-Range Backscatter System

Combining the results from the Noise reduction schemes investigated in **Section 3** and the coding scheme investigated in **Section 4**, an optimal long-range backscatter system can be proposed, and its achievable communication range can be derived given a list of assumptions given by table 6.

The ultimate design will have a backscatter tag design illustrated in figure 12 for modulating the symbol using a DS-SS coding scheme. A unique pseudo-random binary sequence at higher bit rate is used to encode each symbol in the binary data stream. This unique random generator is also assumed known the receiver, such that a matched filter can be designed using the same sequence. At the receiver, the data that is modulated for each bit, will be received and mixed with an LO signal produced by the same local oscillator used for the signal source. This will create a range correlation effect between the two signals, lowering the phase noise in the received signal. The signal will then be low-pass-filtered with a higher filer order to remove any additional harmonic content in the signal. The signal is then passed through a matched filter which is

designed using the same unique pseudo-random binary code used in encoding. The data can finally be decoded using a threshold detector.

Before calculating an achievable range with the system described above, the assumptions that are made in two investigations which can be applied consistently are listed in table 6 below.

| Antenna configuration                     | Monostatic                        |
|---|-----------------------------------|
| Symbol(data) type that can be transmitted | Binary bit data (symbol 0/1 only) |
| Each Symbol Duration                      | 100 $\mu$ s                       |
| Transmit Power, $P_T$                     | 29 dBm                            |
| Antenna Gain at the receiver, $G_{TR}$    | 7 dB                              |
| Antenna Gain at the tag, $G_t$            | 2.1 dB                            |
| Backscatter Transmission Loss $T_b$       | -5 dB                             |
| Carrier frequency, $f_c$                  | 915MHz                            |
| Noise Figure                              | 1.5 dB                            |

Table 6: List of Assumptions for Final Design

There is an inconsistency in assumptions used in our investigations in **Sections 3 and 4** in the bandwidths and offset frequencies used. This is because the simulation in **Section 3** was considered for RFID applications, so realistic parameter values were taken from [6], whereas the investigation in **Section 4** was conducted inspired by the investigation of LoRa backscatter, so values were taken from [1]. The bandwidth and frequency offset values used for **Section 4** were much greater than assumptions used in **Section 3**. Ideally, the discussion should have been conducted using consistent assumptions of offset frequency and bandwidths.

The achievable minimum SNR using DS-SS Coding scheme with harmonic filtering is -23.4 dB using assumptions in table 4 in **Section 4**. If the assumptions were consistent, combining this with Range Correlation Effect, a communication distance of approximately 280m can be achieved using the ‘SNR vs communication range’ graph produced in figure 9 in **Section 3**. The achievable operation range will be increased greater than 280m if the model in section 3 accommodates parameter assumptions used for **Section 4**. Although the phase noise level will be unchanged, the increased bandwidth will increase the received power, allowing for a greater communication range. Future work can be conducted to simulate the spreadsheet modeling with wider bandwidth and higher offset frequencies for a compatible combined-system simulation to achieve a scalable range to 480m achieved in [1].

## 6. Conclusion

In this project, two investigations were conducted with the aim to find solutions to issues which limit the communication range of backscatter communication. Firstly, the problem of oscillator phase noise in monostatic backscatter systems was addressed, and two noise reduction schemes were simulated using a excel spreadsheet models. The two schemes investigated were Range Correlation Effect and Harmonic Backscatter. The performances of implementing the two schemes were compared with a typical monostatic backscatter system which was used as a control. In comparing the achievable ranges achieved from a simulated plot of SNR vs Range, it was concluded that both noise reduction schemes outperform a typical model used as the control. Further, RCE outperformed harmonic backscatter by doubling the achievable range at a typical minimum SNR of 6dB for a monostatic RFID. Considering the difficulty in increasing the communication range, this factor is considered a huge difference, validating the performance of a RCE backscatter system.

In the second part of the project, two coding schemes, CSS and DS-SS were used to modulate the data at the backscatter tag, and a backscatter system design was presented for realistic deployment. Built Simulations using MATLAB were used to find the SNR vs BER plots, and performances of the two coding schemes were compared. It was found that DS-SS outperformed CSS by a decreased required SNR value of 3dB for a BER of  $10^{-3}$ . This is equivalent to an increased communication range by a factor of 1.12, which is also considered significant improvement in range.

Further, to observe the effect of filtering out the higher order harmonic content in the signal created by rapid backscatter switching, a Low pass filter was implemented by option at the receiver. The effect of filtering the harmonic content was evaluated for both coding schemes. It was found that for both coding schemes, filtering out the harmonic content improved BER performance. DS-SS appeared to have a higher susceptibility to harmonics, while CSS was resistant to the harmonic content. Especially for DS-SS, a decrease in almost 2dB SNR for a BER of  $10^{-3}$  was achieved by suppressing the harmonics, which is also a notable improvement in communication range.

Finally, an ultimate backscatter communication design was proposed combining the architectures found optimal in both parts of the project. A DS-SS encoded backscatter system which exploits RCE at the reader is presented. Although consistency is lacked in the channel bandwidth and frequency offset assumptions used between two parts of the project, an approximate achievable range can be arrived at for the ultimate proposed design. A communication range of at least 280m is expected to be achievable given assumptions.

## 7. Future work

In the future, an investigation would be conducted to calculate the correct achievable communication range using consistent assumptions between **Sections 3 and 4**. The achieved range would then be compared to other theoretical and experimental researches found using similar model assumptions. Consistency on the parameters used in modelling would be cross-checked for validity for realistic hardware implementation. Further, physical experiments could be carried out to validate our conclusions found.

Further investigation can be conducted in investigation of the harmonic-tag backscatter model. Instead of exploiting the second harmonic to modulate the data in uplink transmission, even higher order harmonics could be investigated to see if performance can be improved. Moreover, ways of reducing the phase noise by using further different system architectures could be explored such as Bistatic or Ambient Backscatter. For Bistatic, more design parameters could be introduced, such as antenna configuration and antenna placement, which can be manipulated to increase the range.

In **Section 4**, the simulation in our project was conducted to encode only one symbol at a time. In the future, the simulation would be extended to be able to simulate the process of transmitting and receiving of data streams rather than individual symbols. Then, a more accurate conclusion regarding the harmonic content and achievable range can be arrived at.

Further, the investigation on FSCSS (LoRa CSS) can be continued. The decoding method of cyclically shifted symbols is to be found and implemented, considering the problem arisen from attempting to implement a simple correlator for operation.

Moreover, the reason behind presenting a harmonic cancellation mechanism in [1] was because of interference problems arising when allowing multiple-user access. In chirp modulation, different users are each allocated different channel bandwidth. Therefore, the presence of higher order harmonics will be detrimental to performance when multi-user interference is to be considered. By studying the harmonic cancellation scheme proposed in [1] in more detail, the proposed harmonic cancelling which can be done at the backscatter switch can be modelled, rather than simply applying a low pass filter at the receiver as done in the project, which unnecessarily throws away a lot of useful power.

Further, validation could have been carried out to verify that decoding is only possible when the modulation codes were known at the receiver. For example, in DS-SS coding, a different random signal could be passed through the system, and this couldn't have been decoded by the original matched filter coded with a different sequence, validating the improved security advantage that random codes have over CSS.

For the random binary coding scheme, other pseudo-random coding sequences can be studied to be implemented to compare their performances, rather than

generating an arbitrary random sequence using a MATLAB **randi** function as we have used in the project. In particular, gold codes could be investigated, which have bounded small cross-correlations within a set, is known to be useful when allowing multiple-user access in the same frequency range.

## Appendix A: Additional Figures

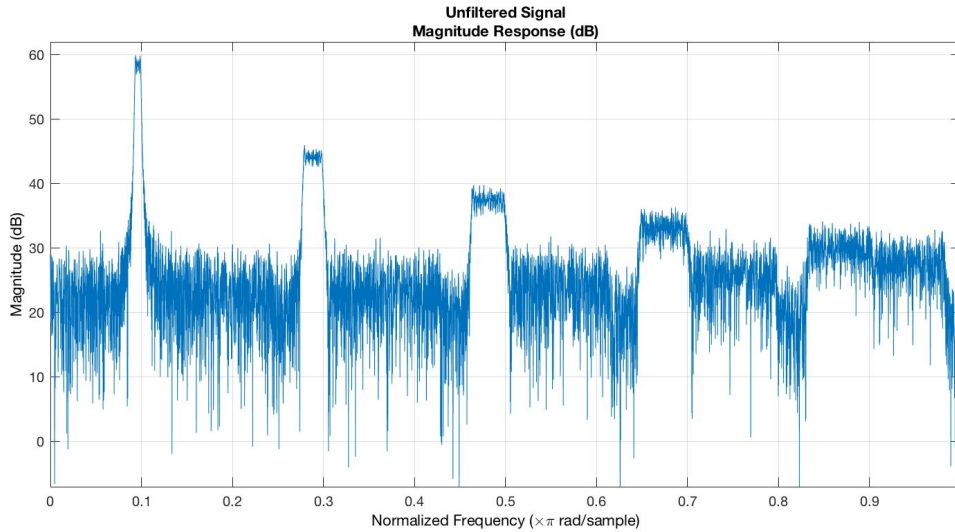


Figure 46. Magnitude frequency Response plot of Unfiltered CSS-modulated symbol, illustrating the presence of higher order harmonics in the data

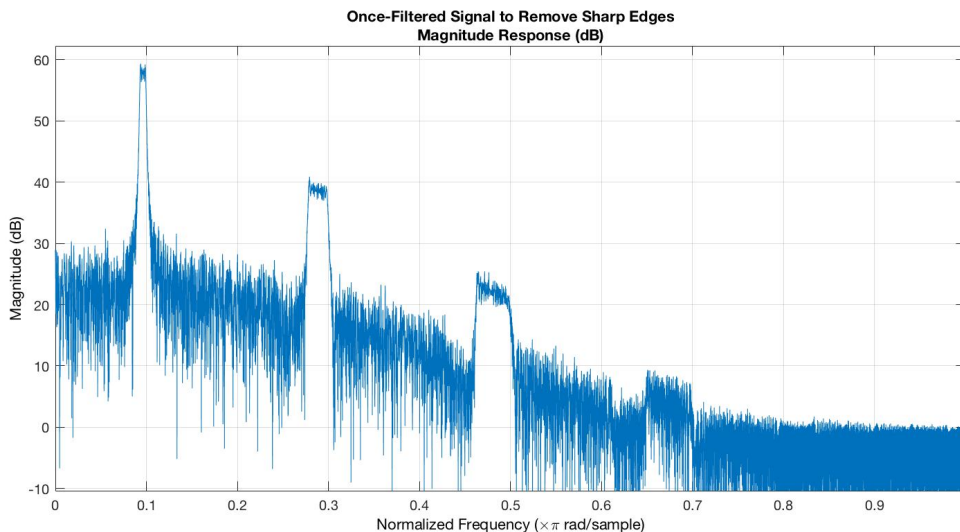


Figure 47. Magnitude frequency Response plot of CSS-modulated symbol after the 1<sup>st</sup> LPF, illustrating the presence of higher order harmonics in the data

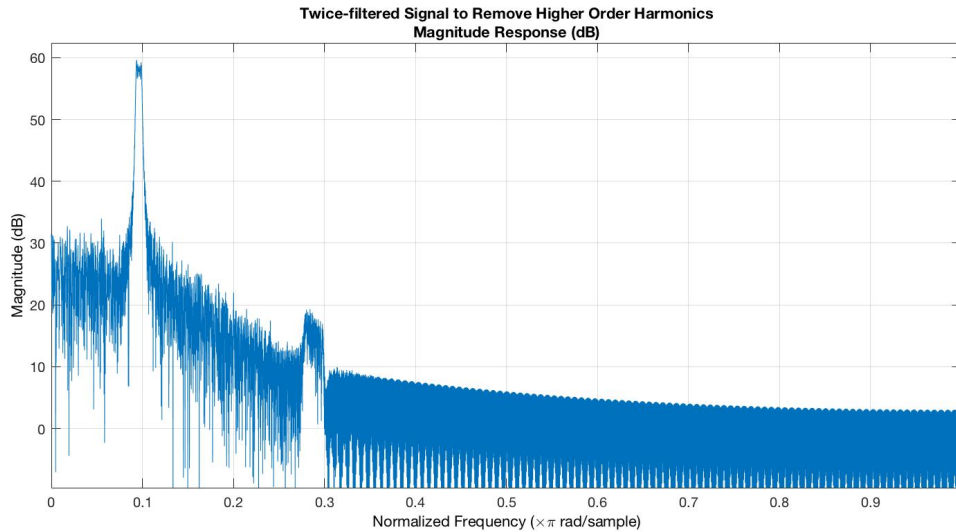


Figure 48. Magnitude frequency Response plot of harmonics-supressed CSS-modulated symbol using 2<sup>nd</sup> LPF, illustrating the effect of filtering

## Appendix B: Covid-19 Disruption

In Section 4 simulation, CUED central linux system would have been used if not for Covid. Time was wasted trying to get remote CPU access, and ultimately simulation was done 3-4 weeks later than expected, near Easter term.

Otherwise, the project was directed since the beginning of Michaelmas, and aimed to be all simulation-based so no other disruptions were made due to Covid-19.

## References

- [1] University of Washington, 2017 *Lora Backscatter: Enabling The Vision of Ubiquitous Connectivity*, <https://dl.acm.org/doi/10.1145/3130970>
- [2] Niu, Li, 2019 *An overview of Backscatter Communications*, <https://ieeexplore.ieee.org/document/8917868>
- [3] Griffin, Durgin, 2009, *Complete Link Budgets for Backscatter-Radio Communications*, <https://ieeexplore.ieee.org/document/5162013>
- [4] Jang, Yoon, 2008, *Range Correlation Effect on the Phase Noise of a UHF RFID Reader* <https://ieeexplore.ieee.org/document/4686748>
- [5] Cornell University, Ma, 2016, *Indoor Locating by Broadband Harmonic RF Backscatter*, <https://ecommons.cornell.edu/handle/1813/44403>
- [6] Budge, Burt, 1993, *Range Correlation Effects on phase noise and Amplitude Noise*, <https://ieeexplore.ieee.org/document/465731>
- [7] Huynh, Hoang, Lu, Niyato, Wang *Ambient Backscatter Communications: A Contemporary Survey* <https://arxiv.org/pdf/1712.04804.pdf>
- [8] D. M. Dobkin, *The RF in RFID: Passive UHF RFID in Practice*
- [9] Ding *Harmonic suppression in frequency shifted backscatter communication*  
<https://ieeexplore.ieee.org/stamp/stamp.jsp?tp=&arnumber=9146880>
- [10] Ma, Hui, Kan *Harmonic WISP: A Passive Broadband Harmonic RFID Platform* <https://ieeexplore.ieee.org/stamp/stamp.jsp?tp=&arnumber=7540224>
- [11] Burt, Budge *Range Correlation Effects on Phase Noise Spectra*  
<https://ieeexplore.ieee.org/stamp/stamp.jsp?tp=&arnumber=522829>
- [12] Liu, Wang, Dou, Zhong *Coding and detection Schemes for Ambient backscatter Communication Systems*  
<https://ieeexplore.ieee.org/stamp/stamp.jsp?tp=&arnumber=7873313>
- [13] Doerry, *Generating Nonlinear FM Chirp Waveforms for Radar*  
<https://core.ac.uk/download/pdf/71305516.pdf>
- [14] Ben-jabeur, Kadri, Hazaa *Enhancing Passive UHF RFID Backscatter Energy Using Chrip Spread Spectrum Signals and Channel Shortening*  
<https://ieeexplore.ieee.org/stamp/stamp.jsp?tp=&arnumber=7565097>
- [15] Budge, Burt *Range Correlation Effects on Radars*  
<https://ieeexplore.ieee.org/stamp/stamp.jsp?tp=&arnumber=270463>
- [16] Baran, Kasal *Oscillator Phase noise models*  
<https://ieeexplore.ieee.org/stamp/stamp.jsp?tp=&arnumber=4542705>
- [17] Ding *Harmonic Suppression in Frequency Shifted Backscatter Communications*

<https://ieeexplore.ieee.org/stamp/stamp.jsp?tp=&arnumber=9146880>

[18] Kim, Kim ***optimum MCS for high-throughput long-range ambient backscatter*** communication networks

<https://ieeexplore.ieee.org/document/8227716>

[19] UC Berkley, ***Passband wireless communication***

[https://inst.eecs.berkeley.edu/~ee121/sp08/handouts/lecture16\\_ece461.pdf](https://inst.eecs.berkeley.edu/~ee121/sp08/handouts/lecture16_ece461.pdf)

[20] University of York ***Equivalent Baseband, Getting started with Communications Engineering***

[https://www-users.york.ac.uk/~dajp1/Introductions/GSW\\_Equivalent\\_Baseband.pdf](https://www-users.york.ac.uk/~dajp1/Introductions/GSW_Equivalent_Baseband.pdf)

[21] Othman, Belz, Boroueny ***Performane Analysis of Matched Filter Bank for Detection of Linear Frequency Modulated Chirp Signals***

<https://ieeexplore.ieee.org/stamp/stamp.jsp?tp=&arnumber=7809103>

[22] ***the Scientist and Engineer's guide to digital Signal Processing***

[https://users.dimil.uniud.it/~antonio.dangelo/MMS/materials/Guide\\_to\\_Digital\\_Signal\\_Process.pdf](https://users.dimil.uniud.it/~antonio.dangelo/MMS/materials/Guide_to_Digital_Signal_Process.pdf)

[23] Marquet, Montavont, Papadopoulos ***Investigating Theoretical Performance and Demodulation Techniques for LoRa***

<https://ieeexplore.ieee.org/document/8793014>

[24] Bae, Kim, Jeon, Jung, Park, Jang ***Analysis of phase noise requirements on local oscillator for RFID system considering range correlation***

<https://ieeexplore.ieee.org/document/4405018>

[25] Hanif ***Frequency-Shift chrip Spread Spectrum Communications with Index Modulation***

<https://arxiv.org/pdf/2102.04642.pdf>

[26] Tao, Zhong, Lin, Zhang ***Symbol Detection of Ambient Backscatter Systems with Manchester Coding***

<https://arxiv.org/pdf/1804.03512.pdf>

[27] Saic, Maletic, ***Random Binary Sequences in Telecommunications***

[http://iris.elf.stuba.sk/JEEC/data/pdf/4\\_113-04.pdf](http://iris.elf.stuba.sk/JEEC/data/pdf/4_113-04.pdf)

[28] Abbas, Awais, Haq ***Comparative analysis of wideband communication techniques: Chirp spread spectrum and direct sequence spread spectrum***

<https://ieeexplore.ieee.org/document/8346348?denied=>

[29] Kanirkar, Saraiya ***BER VS SNR performance Comparisonn of DSSS-CDMA FPGA Based Hardware with AWGN, Spreading Codes & Code Modulation Techniques***, [https://www.idc-online.com/technical\\_references/pdfs/electronic\\_engineering/BER%20Vs%20SNR%20Performance%20Comparison%20of%20DSSSCDMA%20FPGA%20Based%20Hardware.pdf](https://www.idc-online.com/technical_references/pdfs/electronic_engineering/BER%20Vs%20SNR%20Performance%20Comparison%20of%20DSSSCDMA%20FPGA%20Based%20Hardware.pdf)

[30]: Noreen, Bounceur, Clavier ***A study of LoRa low power and wide area network topology***

<https://ieeexplore.ieee.org/document/8075570>

[31]: M.H. Ullah, A.U. Priantoro and M.J. Uddin, “*Design and construction of direct sequence spread spectrum CDMA transmitter and receiver,*” Computer and Information Technology, ICCIT 2008, pp.

[32]: Mane, Kumari, Vamsdhar, Kartheek, Kumar, Rao *Direct Sequence Spread Spectrum Transmission and Reception using Compression Techniques*

<https://ieeexplore.ieee.org/stamp/stamp.jsp?tp=&arnumber=7225439>